

AD-A179 209



EFFECTS OF CORONA ON HEAT  
TRANSFER IN AN ENCLOSURE

THESIS

Donald D. Dyer, Jr.  
Captain, USAF  
AFIT/GA/AA/86D-4

This document has been approved  
for public release and sale; its  
distribution is unlimited.

DEPARTMENT OF THE AIR FORCE  
AIR UNIVERSITY

**AIR FORCE INSTITUTE OF TECHNOLOGY**

Wright-Patterson Air Force Base, Ohio

PII Redacted

87 4

16 059

AFIT/GA/AA/86D-4

EFFECTS OF CORONA ON HEAT  
TRANSFER IN AN ENCLOSURE

THESIS

Donald D. Dyer, Jr.  
Captain, USAF  
AFIT/GA/AA/86D-4

Approved for public release; distribution unlimited

APR 17 1987

A

AFIT/GA/AA/86D-4

EFFECTS OF CORONA ON HEAT  
TRANSFER IN AN ENCLOSURE

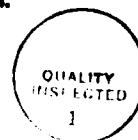
THESIS

Presented to the Faculty of the School of Engineering  
of the Air Force Institute of Technology  
Air University  
In Partial Fulfillment of the  
Requirements for the Degree of  
Master of Science in Astronautical Engineering

Donald D. Dyer, Jr., B.S., M.S.M.

Captain, USAF

December 1986



AFIT/GA/AA/86D-4	
1. TITLE	<input checked="" type="checkbox"/>
2. AUTHOR	<input type="checkbox"/>
3. SUBJECT	<input type="checkbox"/>
4. ABSTRACT	<input type="checkbox"/>
5. INDEXING	<input type="checkbox"/>
6. EVALUATION	<input type="checkbox"/>
7. RECOMMENDATION	<input type="checkbox"/>
8. DISTRIBUTION	<input type="checkbox"/>
9. OTHER	<input type="checkbox"/>
A-1	

Approved for public release; distribution unlimited

## Preface

The purpose of the study was to determine if corona wind enhances heat transfer rates within an enclosure. Numerous studies have been conducted concerning electrostatic cooling. However, there has been very little work which considered how effective electrostatic cooling might be for an enclosed cavity. I chose to study this effect because it was an area of research that was new and, perhaps, I would be able to make a meaningful contribution.

This area of study is wide open for additional research. During my study I found that there are many unanswered questions in this field which need further attention. I have suggested some testing ideas at the end of this report which might help provide answers to those questions. I encourage anyone interested in electrostatics or heat transfer to pursue the topic I have chosen. There are numerous opportunities to make a truly original contribution to the field.

This thesis could not have been completed were it not for the help of several very special people. First, I would like to thank my advisor, Professor Milton Franke, for suggesting this topic and providing timely advice and encouragement. I wish to express my thanks to Professors James Hitchcock and William Elrod for their help. Special thanks also go to the AFIT fabrication shop, headed by Mr. Carl Shortt, and the technicians of the Astronautical Engineering Department, under the direction of Mr. Nicholas Yardich. I would like to especially recognize Mr. Jay Anderson for his enormous help in setting up the tests. Most of all, I want to express my

gratitude to my wife Deborah and my son David. They contributed more than they realize with their loving encouragement, understanding, and patience.

Donald D. Dyer, Jr.

## Table of Contents

	<u>Page</u>
Preface.....	i
List of Figures.....	v
List of Symbols.....	vii
List of Tables.....	x
Abstract.....	xi
I. Introduction.....	1
Background.....	1
Objective.....	3
Approach.....	3
II. Experimental Apparatus.....	4
Rectangular Cavity.....	4
Heating System.....	5
Cooling System.....	7
High Voltage System.....	7
Interferometer.....	8
III. Theory.....	9
Heater Plate System.....	9
Enclosed Cavity System.....	11
IV. Test Procedures.....	13
Corona Heat Transfer Tests.....	14
Energy Balance Tests.....	15

	<u>Page</u>
V. Results and Discussions.....	17
Energy Balance Tests.....	17
Corona Tests.....	20
VI. Conclusions.....	37
VII. Recommendations.....	38
References.....	39
Appendix A: Tabulated Data.....	42
Appendix B: Photographs of Test Equipment.....	52
Appendix C: Interferometer Alignment.....	59
VITA.....	63

## List of Figures

<u>Figure</u>	<u>Page</u>
1. Depiction of Phenolic Cavity With Corona Wires, Heater Plates, Water Jacket, and Terminals.....	5
2. Top View of Hot/Cold Phenolic Surface Showing Thermocouple Placements.....	6
3. Control Volume Defining Heater Plate System.....	9
4. Control Volume Defining Enclosed Cavity System.....	12
5. Front View of Test Cavity Showing Charge on Corona Wires for Each Test Configuration.....	13
6. Thermocouple Locations on Fiberglass Surfaces (Top/Bottom View).....	15
7. Thermocouple Locations on Fiberglass Surfaces (Side View).....	16
8. Thermocouple Locations on Bakelite and Glass Surfaces (End View).....	16
9. Flow Patterns Resulting From Positive Voltage Potential for Configuration #1.....	23
10. Flow Patterns Resulting From Negative Voltage Potential for Configuration #1.....	24
11. Flow Patterns Resulting From Positive Voltage Potential for Configuration #2.....	26
12. Flow Patterns Resulting From Negative Voltage Potential for Configuration #2.....	26
13. Flow Patterns Resulting From Positive Voltage Potential for Configuration #3.....	28



<u>Figure</u>	<u>Page</u>
14. Flow Patterns Resulting From Negative Voltage Potential for Configuration #3.....	29
15. Flow Patterns Resulting From Positive Voltage Potential for Configuration #4.....	31
16. Flow Patterns Resulting From Negative Voltage Potential for Configuration #4.....	31
17. $Q_{cav}$ vs. Voltage for Configuration #1.....	33
18. $Q_{cav}$ vs. Voltage for Configuration #2.....	34
19. $Q_{cav}$ vs. Voltage for Configuration #3.....	35
20. $Q_{cav}$ vs. Voltage for Configuration #4.....	36
21. Photograph of Test Object.....	53
22. Picture of High Voltage Power Supply.....	54
23. Picture of Transformer Used to Adjust Heater Plate Current.....	55
24. Photograph of Digital Scanner for Thermocouples.....	56
25. Photograph of Temperature Measuring Unit Used to Take Thermocouple Readings.....	57
26. Picture of Digital Multimeter Used to Measure Heater Plate Currents.....	58
27. Mach-Zehnder Interferometer.....	62

### List of Symbols

A	-	Surface area ( $\text{ft}^2$ )
h	-	Convective heat transfer coefficient ( $\text{BTU/hr-ft}^2\text{-}^\circ\text{F}$ )
I	-	Heater plate current (amps)
k	-	Thermal conductivity ( $\text{BTU/hr-ft-}^\circ\text{F}$ )
P	-	Heater power ( $\text{BTU/hr}$ )
Q	-	Heat transfer rate ( $\text{BTU/hr}$ )
R	-	Resistance of heater plate wires (ohms)
T	-	Temperature ( $^\circ\text{F}$ )
$\Delta X$	-	Thickness of material (ft)
$\sigma$	-	Stefan-Boltzmann constant ( $\text{BTU/hr-ft}^2\text{-}^\circ\text{R}^4$ )
$\epsilon$	-	Emissivity of the material (dimensionless)

### List of subscripts

amb	-	Ambient condition
b	-	Bakelite surface
(c)	-	Conduction or convection
cav	-	Cavity formed by phenolic surfaces
f	-	Horizontal fiberglass surface adjacent to heater plates
fh	-	Outer fiberglass surface corresponding to side with heater plates
fhs	-	Outer fiberglass surface corresponding to side of heater plates
fs	-	Outer fiberglass surface corresponding to side of cavity
ft	-	Horizontal fiberglass surface adjacent to water jacket
g	-	Optical glass
gi	-	Inside surface of optical glass
go	-	Outside surface of optical glass
he	-	End of heater plates
htr	-	Heater plates
pc	-	Cooled phenolic surface inside cavity

ph	-	Heated phenolic surface inside cavity
ps	-	Phenolic surface on side of cavity
(r)	-	Radiation
w	-	Water in water jacket

### List of Tables

<u>Table</u>	<u>Page</u>
I. Parameters Used in Convection and Conduction Equation for Energy Balance Test (Heating From Below).....	18
II. Parameters Used in Radiation Equation for Energy Balance Test (Heating From Below).....	19
III. Parameters Used in Convection and Conduction Equation for Energy Balance Test (Heating From Above).....	19
IV. Parameters Used in Radiation Equation for Energy Balance Test (Heating From Above).....	20
V. Average Temperatures ( $^{\circ}\text{F}$ ) for Configuration #1.....	21
VI. $Q_{\text{cav}}$ Rates for Configuration #1.....	22
VII. Average Temperatures ( $^{\circ}\text{F}$ ) for Configuration #2.....	24
VIII. $Q_{\text{cav}}$ Rates for Configuration #2.....	25
IX. Average Temperatures ( $^{\circ}\text{F}$ ) for Configuration #3.....	27
X. $Q_{\text{cav}}$ Rates for Configuration #3.....	27
XI. Average Temperatures ( $^{\circ}\text{F}$ ) for Configuration #4.....	29
XII. $Q_{\text{cav}}$ Rates for Configuration #4.....	30

## Abstract

Experiments were conducted to determine the effects of corona wind on heat transfer rates for enclosures. Tests were performed with an enclosed cavity heated on the bottom and cooled on the top (and vice-versa). A corona wind was established inside the cavity by applying high voltages to 0.004 inch diameter chromel wires placed along the hot and cold surfaces of the cavity. Tests were conducted using both positive voltage potential and negative voltage potential to create the corona discharge. Different wiring configurations were used to establish a variety of flow patterns inside the cavity.

The heated surface heat transfer rates were calculated for each of the test configurations with and without corona. These heat transfer rates were determined when the corona discharge was present and compared to the rates found when the discharge was not present. Comparing these transfer rates revealed how much the corona wind augmented the heat transfer process. Results showed corona wind can increase heat transfer rates inside an enclosure by almost four times the rates attained without the corona discharge for the wire configurations investigated.

# EFFECTS OF CORONA ON COOLING FOR AN ENCLOSURE

## 1. Introduction

When an intense electric field is applied to a very thin wire, the fluid near the wire becomes ionized. Since these ions have the same charge as the wire, a flow is created as these ions move from the charged pole to ground. As the ions move through the fluid they collide with neutral molecules producing a low velocity flow within the fluid known as the corona or electric wind. This induced flow has proven to increase free convection heat transfer rates up to eight times the rate without the electric field (1:44). This paper investigates the effect of electrostatic cooling in a rectangular enclosure.

## Background

Numerous studies have shown that corona wind can enhance convective heat transfer rates. One of the first to discover this effect was Senftleben (2) who revealed his discovery in the early 1930's. Although there were a few patents developed from this concept (3,4), serious study did not begin to flourish until the 1960's.

The studies of the 1960's provided much of the groundwork for electrostatic cooling theory which continues to the present. One of the

early pioneers was Velkoff (5-10) who studied flat plates, channel flows, and other configurations using electrostatic cooling. O'Brien (11) showed how pressure and working fluid composition effected electrostatic cooling. Franke (12,13) showed the flow patterns, induced by an electrostatic field around a vertical flat plate and a vertical cylinder. The paper by Velkoff and Kulacki (14) provides a review of previous work done in the field of electrostatic cooling.

Ostrach (15) presents a review of heat transfer studies in enclosures. Many of the studies on rectangular enclosures have considered the case of heat transfer with the vertical side walls maintained at different temperatures. Batchelor (16,17) studied this configuration and found the effect of Rayleigh number and height-to-width ratios on internal flows. He concluded that for small Rayleigh numbers, or large height-to-width ratios, most of the heat was transferred by conduction (i.e. convection was negligible). Wilkes (18) studied a square enclosure heated on a vertical wall and cooled on the opposite wall for a Rayleigh number on the order of  $10^5$ . His numerical analysis revealed the isotherms were essentially horizontal lines away from the vertical boundary layers and showed the existence of a relatively stagnant core. Experiments by Elder (19) confirmed the stagnant core hypothesis. A numerical study by Vahl Davis (20) also showed horizontal isotherms in heated enclosures with small Rayleigh numbers.

Although there have been numerous studies on electrostatic cooling and heat transfer in enclosures, little work has been done in an attempt to consider the effect of electrostatics on heat transfer in enclosures.



### Objective

The objective of this research was to determine experimentally the effect of a corona wind on the convective heat transfer rate within a rectangular enclosure with optical glass at each end. An interferometer was used to provide qualitative data to determine the types of flow patterns developed by different heater configurations and corona intensities. The change in heat transfer rates due to the corona was determined by comparing the heat transfer rates with and without a corona wind inside the enclosure.

### Approach

The enclosed cavity was heated from above or below (depending on the configuration being tested) and the heat transfer rate into the cavity was calculated from temperature measurements during tests under steady-state conditions. The heat conducted from the heater plates into the cavity was used as the baseline from which comparisons in the heat transfer rate were made for tests with and without the corona discharge present in the cavity. When corona discharge was established inside the enclosure, the temperature of the heated plate was reduced. The temperature drop was attributed to corona wind cooling. Heat transfer equations were used to calculate the heat transfer rates and an energy balance was used to ensure all energy losses were considered.

## II. Experimental Apparatus

The overall effect of corona discharge on the heat transfer rates inside a rectangular cavity with a square cross section was studied with the aid of several pieces of equipment. The equipment may be grouped into five categories: 1) rectangular cavity, 2) heating system, 3) cooling system, 4) high voltage supply, and 5) interferometer. Because of the high voltages involved in this experiment, insulating materials were chosen whenever possible. Details about each of these categories are described in the paragraphs that follow.

### Rectangular Cavity

The walls of the rectangular cavity were made from 5/16 in thick phenolic (Insurok) plates. The phenolic plates were assembled into a 4 x 4 x 10 1/2 in cavity, Fig. 1. The four sides of the cavity were attached with nylon screws so the upper and lower plates could be easily removed for modifications. Three corona wires (0.004 in dia., Chromel) were spaced 1 in apart along the top and bottom surfaces inside the cavity. Bolts were used as terminals to connect the corona wires to the high voltage source. Bakelite plates (4 x 1 x 1/8 in) were used to insulate the high voltage terminals from the metallic heater plates and water jacket. Eight Type J (iron-constantan) thermocouples were used to measure the temperature of the top and bottom cavity surfaces. The thermocouples were positioned in holes (1/32 in dia.) drilled into the back of the top and bottom phenolic plates to within 1/32 in from the inside surface. The thermocouple readings were used to estimate an average plate temperature for the hot and

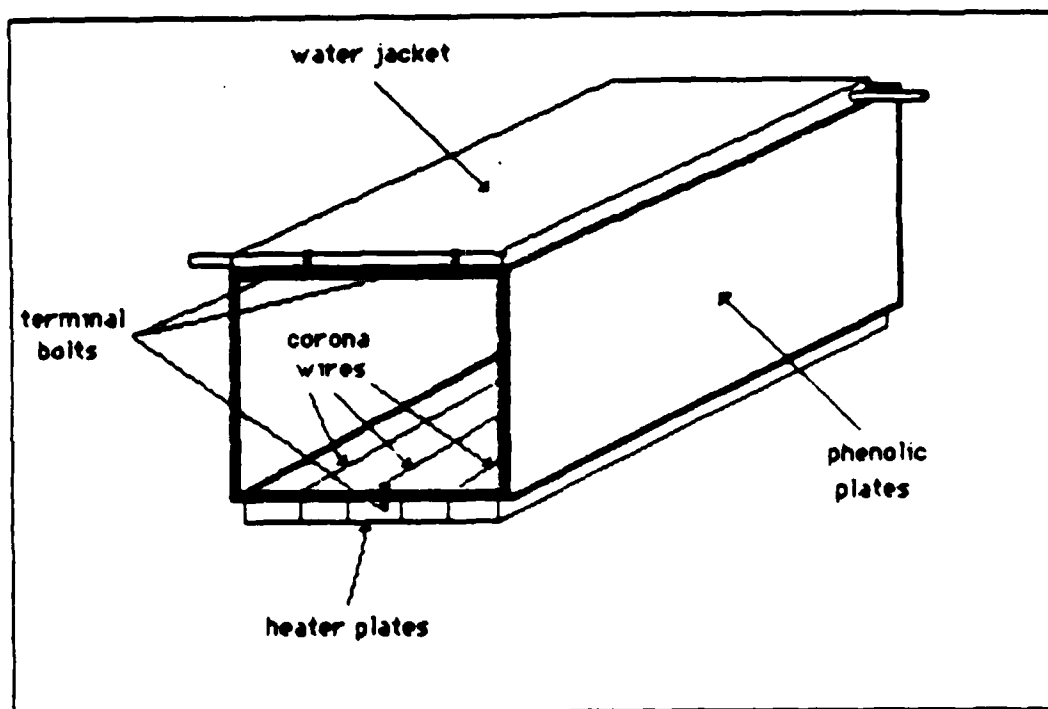


Fig. 1. Depiction of Phenolic Cavity With Corona Wires, Heater Plates, Water Jacket, and Terminals

cold cavity surfaces, Fig. 2. The cavity was enclosed at both ends by  $1/4$  in optical glass. The glass pieces were placed in plexiglass bulkheads which attached to the ends of the cavity with plexiglass clamps and nylon screws. The entire cavity was wrapped with fiberglass insulation to minimize heat losses through the side plates of the cavity.

### Heating System

A set of five heater plates, Fig. 1, was attached to the outside surface of the phenolic cavity and used as the heat source. Each heater plate was 10 in long and  $3/4$  in wide and used nichrome wire as the heating element.

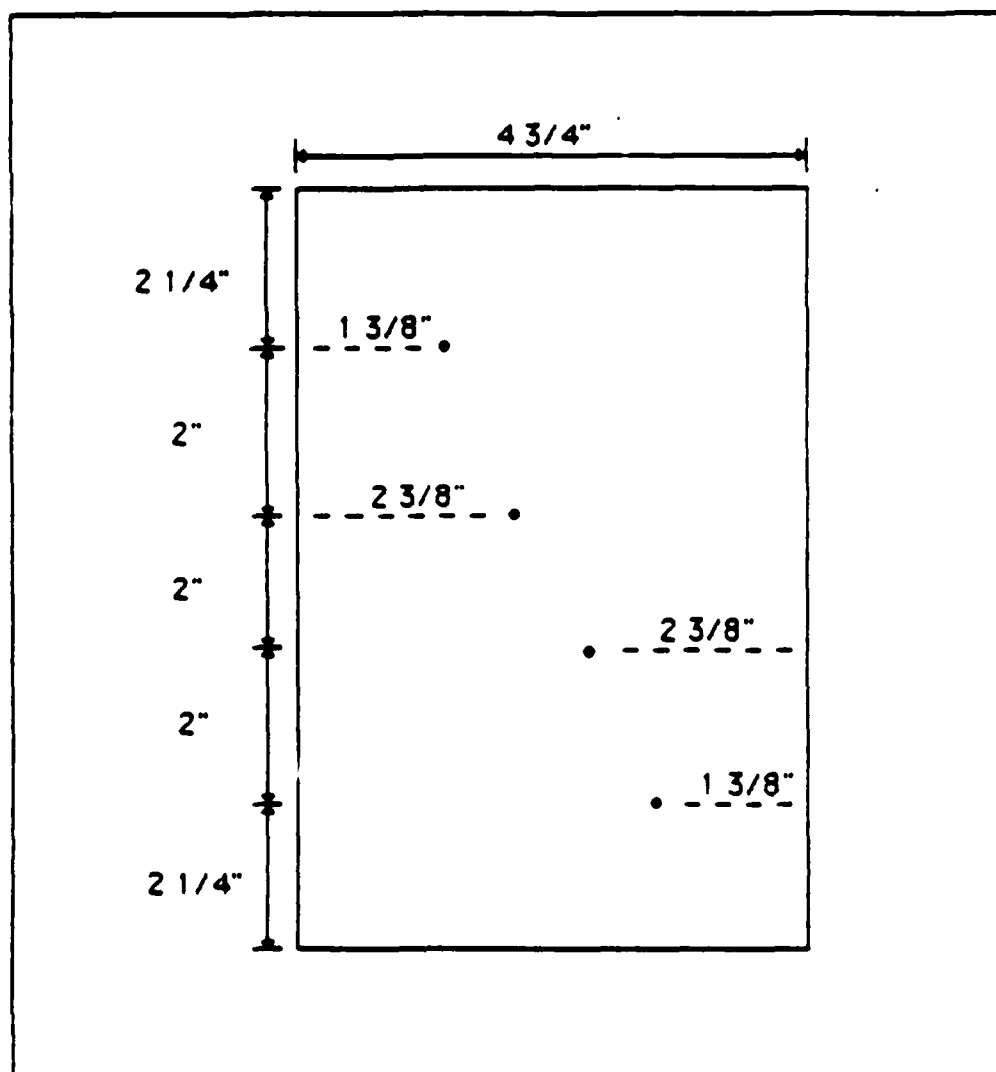


Fig. 2. Top View of Hot/Cold Phenolic Surface Showing Thermocouple Placements

The heater plates were held together by a piece of phenolic and each plate had its own electrical outlet. Two plexiglass U-joints (1 in wide and  $\frac{3}{4}$  in thick) were used to hold the heater plates against the test cavity. The power to the heater was controlled by a transformer which provided the ability to adjust the heater power. The heater plate wires had a resistance of 82.3 ohms. A digital multimeter was used to measure the current applied

to each heater plate. From these readings, the total power applied to the heater plates was determined.

### Cooling System

A copper water jacket was used to provide cooling for the top or bottom surface of the test cavity, Fig. 1. The water jacket was made from 1/16 in thick copper plates 4 in wide and 10 in long. The two plexiglass U-joints used to hold the heaters in place were also used to hold the water jacket against the phenolic outer wall (the wall opposite from the heater plates). Tap water, used as the coolant, was routed through the 1/8 in spacing between the copper plates. Guide vanes, spaced 1 and 1/3 in apart, were used to prevent stagnation of the water inside the water jacket. The water was piped into and out of the water jacket through a plastic hose with a 1/4 in inside diameter and a 1/2 in outside diameter.

### High Voltage System

The high voltage power supply provided the voltage necessary to produce the corona discharge. The corona discharge was formed around the small diameter wires (0.004 in dia., Chromel) which were placed along the inside of the phenolic cavity (see Fig. 1). These wires were connected to high voltage lead wires at metallic terminals. Three wires were placed on both the hot and cold surfaces of the cavity. The power supply is capable of producing up to 30 kilovolts DC with either positive or negative voltage potential.

### Interferometer

A Mach-Zehnder interferometer was used to estimate the flow patterns developed with the different test configurations from the interferometer fringes. The spacing and orientation of the fringes were controlled by adjusting the mirrors. Two 1/4 in optical glass plates were mounted in the reference section to compensate for the optical glass used to enclose the test cavity. A 100 watt mercury vapor lamp was used for the light source. The light was passed through a 77A Wratten filter (5461 Angstroms) to provide monochromatic light. Details of the interferometer alignment are given in Appendix C.

### III. Theory

This research considers the effect corona discharge has on the rate heat is being transferred into the enclosed cavity. In order to study this effect, it is necessary to isolate the primary surface across which heat is being transferred into the cavity. The test apparatus is divided into two separate control volumes, Figs. 3 and 4, to isolate the surface of interest,  $Q_{cav}$ . Under steady-state conditions, for each control volume, the heat transferred in must equal the heat transferred out.

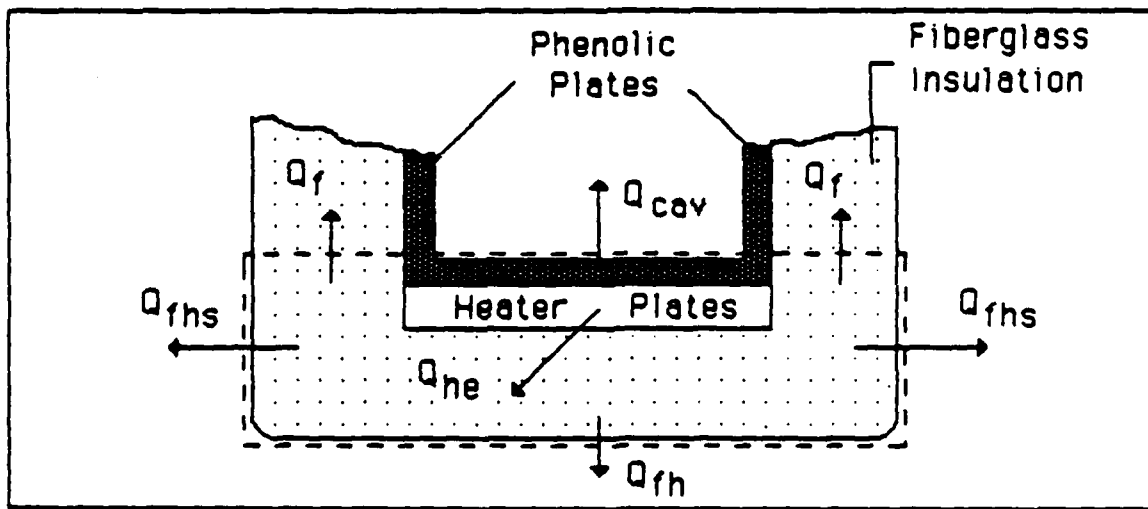


Fig. 3. Control Volume Defining Heater Plate System

#### Heater Plate System

The control volume in Fig. 3 is referred to as the heater plate system. The heat losses from the heater plate system are shown in Fig. 3; therefore,

the total heat transferred out is

$$Q_{out} = 2 (Q_{he(c)} + Q_{he(r)}) + 2 (Q_{rhs(c)} + Q_{rhs(r)}) + (Q_{fh(c)} + Q_{fh(r)}) + 2 Q_f + Q_{cav} \quad (1)$$

The heat transfer rate to the heater plate system is the power applied to the heater plates. The rate energy is supplied to the heaters is

$$Q_{in} = I^2 R \quad (2)$$

Applying an energy balance to the heater plate system (for steady-state conditions) gives

$$Q_{in} = Q_{out} \quad (3)$$

or, substituting from Equations (1) and (2):

$$I^2 R = 2 (Q_{he(c)} + Q_{he(r)}) + 2 (Q_{rhs(c)} + Q_{rhs(r)}) + (Q_{fh(c)} + Q_{fh(r)}) + 2 Q_f + Q_{cav} \quad (4)$$

The terms on the right side of Equation (4) are calculated using the basic heat transfer equations:

$$Q = k A \Delta T / \Delta X \quad (5)$$



$$Q = h A \Delta T \quad (6)$$

$$Q = \sigma \epsilon A (T^4 - T_{amb}^4) \quad (7)$$

where  $Q_{he(c)}$  and  $Q_{cav}$  are calculated from Equation (5);  $Q_{fhs(c)}$  and  $Q_{fh(c)}$  are calculated from Equation (6); and  $Q_{he(r)}$ ,  $Q_{fhs(r)}$ , and  $Q_{fh(r)}$  are calculated from Equation (7). The thermal conductivity for phenolic is 7 times greater than for fiberglass; therefore, most of the heat transfer along the top of the control volume, Fig. 3, is into the cavity and  $Q_f$  is assumed to be negligible. This assumption is proven to be valid in the Results section.

The convection coefficient,  $h$ , in Equation (6), is a function of the orientation of the surface where the convection takes place. Values for  $h$  were obtained from the equation given by Hsu (21:384-385):

$$h = b (T - T_{amb})^{0.25} \quad (8)$$

where  $b$  is 0.20 for a horizontal plate facing downwards, 0.38 for a horizontal plate facing upwards, and 0.28 for a vertical plate less than one foot high.

#### Enclosed Cavity System

The enclosed cavity system and heat transfer rates are illustrated in Fig. 4. The energy balance equation for the cavity system is given by:

$$2 Q_f + Q_{cav} = 2 (Q_{fs(c)} + Q_{fs(r)}) + 2 (Q_{g(c)} + Q_{g(r)}) + 2 Q_{ft} + Q_w \quad (9)$$

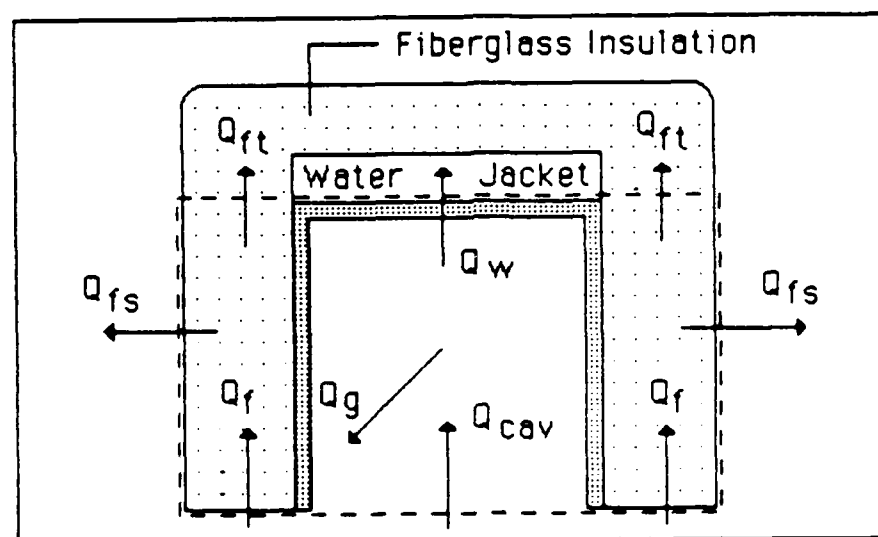


Fig. 4. Control Volume Defining Enclosed Cavity System

Again, the terms on the right side of this equation are determined from the basic heat transfer equations, Equations (5), (6), and (7).  $Q_{cav}$  and  $Q_w$  are calculated from Equation (5);  $Q_{fs(c)}$  and  $Q_{g(c)}$  are calculated from Equation (6); and  $Q_{fs(r)}$  and  $Q_{g(r)}$  are calculated from Equation (7).  $Q_f$  and  $Q_{ft}$  are assumed to be negligible since most of the heat is transferred into the cavity. This is due to the thermal conductivity of phenolic being much greater than fiberglass.

For Equations (4) and (9), if the left side of the equation approximately equals the right side of the equation, then one can assume all of the heat losses are accounted for in each control volume since each term in both equations is calculated independently.

#### IV. Test Procedures

The purpose of the test was to determine the effect of corona wind on the heat transfer rate within an enclosure. Tests were run to determine how different wire configurations and flow patterns affected the heat transfer rate, measured in terms of  $Q_{cav}$ , into the cavity, Fig. 5.

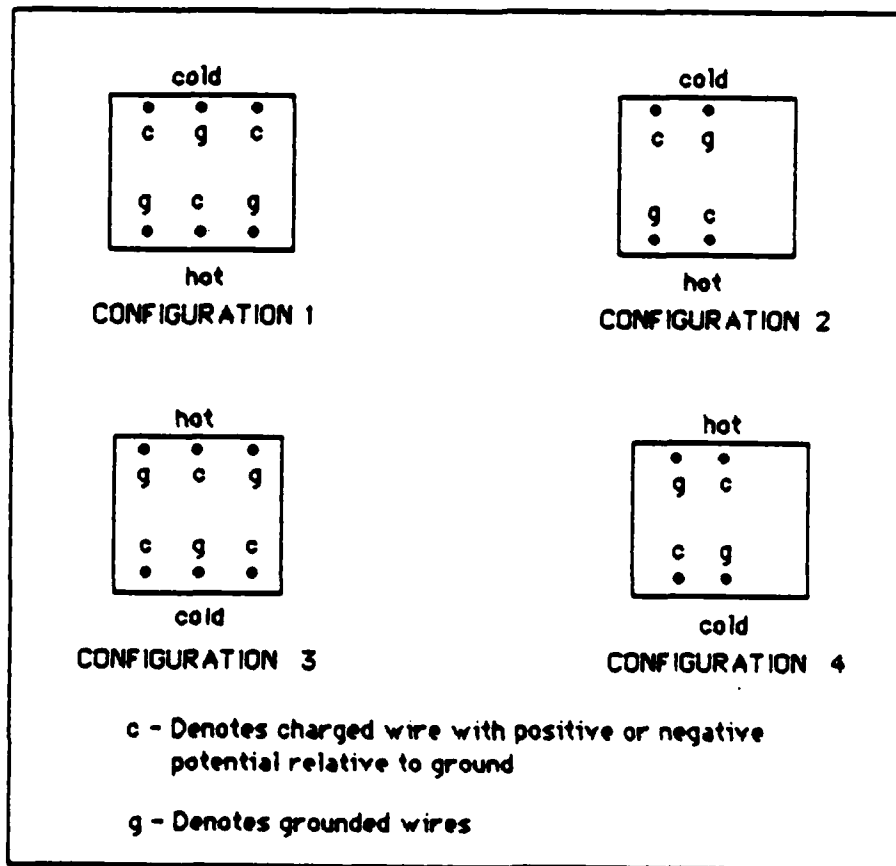


Fig. 5. Front View of Test Cavity Showing Charge on Corona Wires for Each Test Configuration.

The corona wind intensity was varied to determine the effect on the heat transfer rate. Each configuration was tested at 5kV, 8kV, 11kV, and 14kV using a positive as well as a negative voltage potential for a total of 32

test runs.

The thermocouples, with locations shown in Fig. 2, were used to measure the temperature of the hot and cold plates within the cavity (four thermocouples for each plate). The average temperature of each plate was determined from an arithmetic average of the thermocouple readings. The thermocouple leads were connected to a scanner which permitted the temperature readings to be displayed on a digital display unit. To protect the temperature measuring equipment from the high voltage field, both the digital display unit and the scanner were disconnected while the high voltage was applied to the corona wires.

#### Corona Heat Transfer Tests

A steady-state temperature difference of approximately 85 °F was established between the hot and cold surfaces inside the cavity prior to each test. After recording the temperatures of the heated and cooled plates, the temperature measuring equipment was disconnected and the high voltage was applied. The high voltage remained on for 15 minutes to allow the hot and cold surfaces to reach steady-state. Immediately after the high voltage was turned off, the new steady-state temperatures were recorded. The resulting increase in the temperature difference between the hot and cold plates was attributed to the cooling effect of the corona wind on the heated surface while the temperature of the cooled surface was constant. In order to convert this increased temperature difference into an increase in the heat transfer rate, Equation (5) was used to calculate the conduction into the cavity. The conduction rate without the corona discharge was compared to the conduction with the discharge.

The current through each of the five heater plates was measured, in series, along the wires connecting each plate to the power source (transformer). The measurements were made with a digital multimeter, which was disconnected when the high voltage was applied to the corona wires to protect the multimeter.

### Energy Balance Tests

Energy balance tests were performed to be certain that all of the energy lost from the heater plates were accounted for. The losses from the heater plates are depicted in Fig. 3 and Equation (4) was used to determine if the energy put into the heater plates equalled the energy lost. The energy balance tests began by establishing the same steady-state temperature difference (approximately 85 °F), between the hot and cold surfaces, that was used in the corona tests. Once at steady-state, thermocouples were used to measure the temperature at numerous locations around the test section, Figs. 6, 7, and 8, in order to determine accurate average surface temperatures. These measurements were used to account for the heat losses throughout the test apparatus. The energy balance tests were performed for the case of heating from below as well as heating from above.

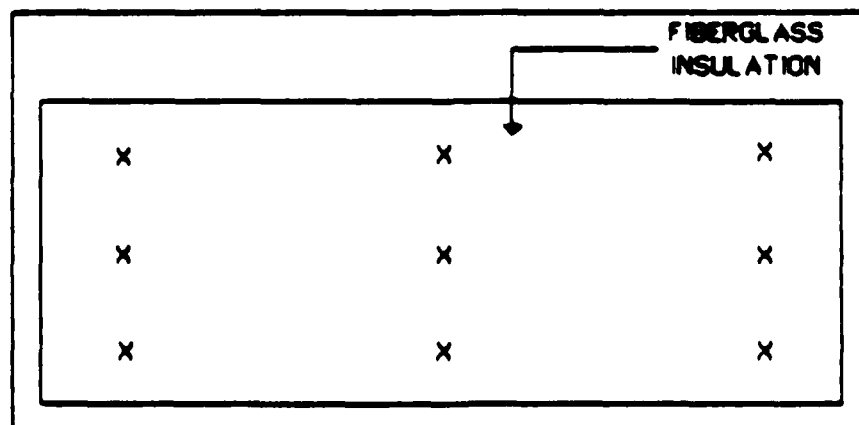


Fig. 6. Thermocouple Locations on Fiberglass Surfaces (Top/Bottom View)

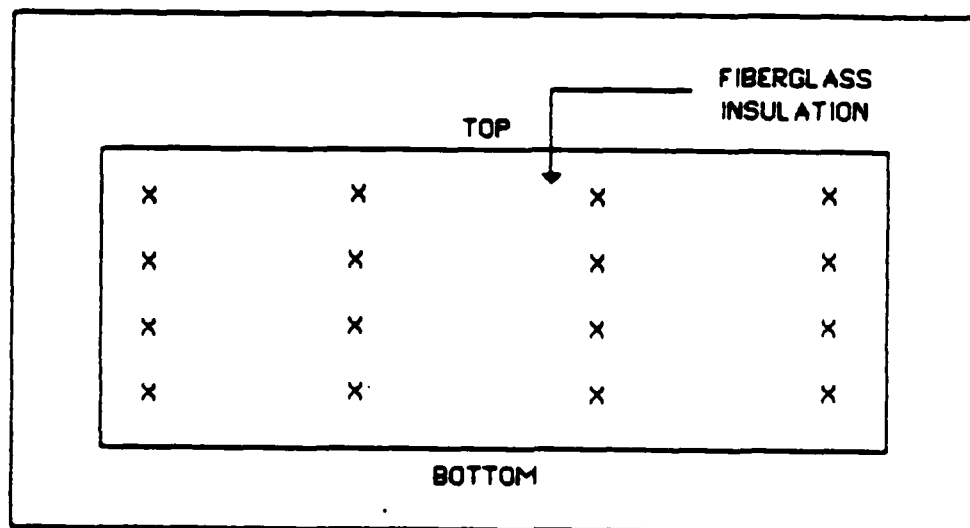


Fig. 7. Thermocouple Locations on Fiberglass Surfaces (Side View)

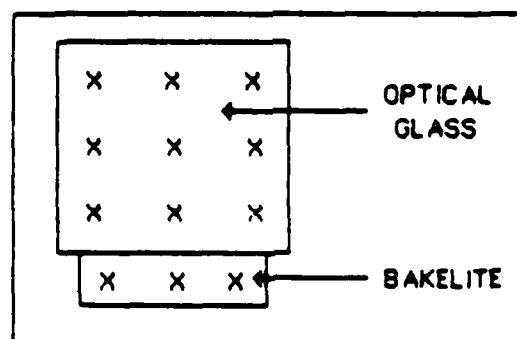


Fig. 8. Thermocouple Locations on Bakelite and Glass Surfaces (End View)

## V. Results and Discussion

The results of the tests are presented in two sections. The first section discusses the energy balance tests and the second section discusses the corona tests. The temperature readings from the corona tests are tabulated in Appendix A of this report and are referenced in the discussions that follow.

### Energy Balance Tests

The purpose of the energy balance tests was to be certain there was a balance between the energy put into the heater plate system (Fig. 3) and the energy lost by the heater plate system. If a balance exists, then one can be reasonably assured that all of the energy losses were accounted for. This is important because the value for  $Q_{cav}$  in Fig. 3 was used as the baseline for the corona tests.

Heating From Below. The first energy balance test was performed while heating the cavity from below. The heater plate current was set to maintain the desired temperature difference between the hot and cold surfaces (approximately 85 °F). The total energy rate input into the the five heater plates was 50.7 BTU/hr, from Equation (2), using a resistance of 82.3 ohms and a current of 0.19 amps. Table I shows the parameters used to calculate the conduction and convection losses using Equations (5) and (6). The losses due to radiation were found by substituting the parameters in Table II into Equation (7). Therefore, from Equation (1), the total rate at which energy is being lost is 42.6 BTU/hr. This is within 16% of the 50.7 BTU/hr rate energy was transferred to the heater plates. Since this percentage is relatively

small, then the assumption that  $Q_r$ , Fig. 3, is negligible is valid.

Heating From Above. The energy balance test for the case of heating from above also produced reasonably accurate results. The heaters required 0.18 amps to maintain the desired temperature difference between the heated and cooled surfaces. Substituting 0.18 amps and 82.3 ohms into Equation (2), the energy input to the heaters was 45.5 BTU/hr. The

TABLE I  
Parameters Used in Convection and Conduction  
Equations for Energy Balance Test (Heating From Below).

	$k, \frac{\text{BTU}}{\text{hr-ft}^2-\text{°F}}$	$\Delta X, \text{ft}$	$h, \frac{\text{BTU}}{\text{hr-ft}^2-\text{°F}}$	$A, \text{ft}^2$	$\Delta T^*, \text{°F}$	$Q^{**}, \frac{\text{BTU}}{\text{hr}}$
$Q_{\text{cav}}$	0.14	0.031	---	0.342	82	12.7
$Q_{\text{rhs(c)}}$	---	---	0.57	0.098	17.1	1.0
$Q_{\text{he(c)}}$	0.13	0.016	---	0.011	39.3	3.5
$Q_{\text{fh(c)}}$	---	---	0.46	0.409	27.9	5.2
$Q_{\text{fs(c)}}$	---	---	0.40	0.342	4.2	0.6
$Q_{\text{g(c)}}$	---	---	0.51	0.111	11.1	0.6
$Q_w$	0.18	0.041	---	0.342	6.3	9.5

\* -  $\Delta T$ 's are defined as follows:

$$\Delta T_{\text{cav}} = T_{\text{htr}} - T_{\text{hc}} \quad \Delta T_{\text{fh(c)}} = T_{\text{fh}} - T_{\text{amb}} \quad \Delta T_{\text{g(c)}} = T_{\text{go}} - T_{\text{amb}}$$

$$\Delta T_{\text{rhs(c)}} = T_{\text{rhs}} - T_{\text{amb}} \quad \Delta T_{\text{fs(c)}} = T_{\text{fs}} - T_{\text{amb}} \quad \Delta T_w = T_{\text{pc}} - T_w$$

$$\Delta T_{\text{he(c)}} = T_{\text{htr}} - T_b$$

\*\* -  $Q$ 's correspond to those shown in the first column.



TABLE II

Parameters Used in Radiation Equation  
for Energy Balance Test (Heating From Below)

	$\epsilon$	A, ft <sup>2</sup>	T <sub>1</sub> , °R	T <sub>2</sub> , °R	Q*, BTU/hr
Q <sub>rh(r)</sub>	0.90	0.409	557.9	530.0	11.3
Q <sub>he(r)</sub>	0.90	0.011	581.8	530.0	0.6
Q <sub>fs(r)</sub>	0.90	0.342	534.2	530.0	1.3
Q <sub>g(r)</sub>	0.95	0.111	541.1	530.0	1.2
Q <sub>rhs(r)</sub>	0.90	0.098	547.1	530.0	1.6

\* - Q's correspond to those shown in the first column.

TABLE III

Parameters Used in Convection and Conduction  
Equations for Energy Balance Test (Heating From Above)

	k, $\frac{\text{BTU}}{\text{hr-ft}^2-\text{°F}}$	$\Delta x$ , ft	h, $\frac{\text{BTU}}{\text{hr-ft}^2-\text{°F}}$	A, ft <sup>2</sup>	$\Delta T^*$ , °F	Q**, $\frac{\text{BTU}}{\text{hr}}$
Q <sub>cav</sub>	0.14	0.031	---	0.342	5.6	8.6
Q <sub>rhs(c)</sub>	---	---	0.55	0.098	14.7	0.8
Q <sub>he(c)</sub>	0.13	0.016	---	0.011	33.5	3.0
Q <sub>rh(c)</sub>	---	---	0.89	0.409	29.8	10.8
Q <sub>fs(c)</sub>	---	---	0.32	0.342	1.7	0.2
Q <sub>g(c)</sub>	---	---	0.50	0.111	10.3	0.6
Q <sub>w</sub>	0.18	0.041	---	0.342	3.2	4.8

\* -  $\Delta T$ 's are defined below TABLE I on p. 18.

\*\* - Q's correspond to those shown in the first column.

conduction and convection losses were found by substituting the values from Table III into Equations (5) and (6). The radiation losses were calculated using the parameters in Table IV and Equation (7). Using Equation (1), the total rate energy was lost was 43.5 BTU/hr which is within 4% of the energy rate input to the heaters. The small difference between energy added to the heaters and losses from the heaters shows all losses were considered and the assumption that  $Q_f$ , Fig. 3, is negligible is valid.

TABLE IV  
Parameters Used in Radiation Equation  
for Energy Balance Test (Heating From Above)

	$\epsilon$	$A, ft^2$	$T_1, ^\circ R$	$T_2, ^\circ R$	$Q^*, BTU/hr$
$Q_{fh}(r)$	0.90	0.409	564.4	534.6	12.5
$Q_{he}(r)$	0.90	0.011	586.7	534.6	0.6
$Q_{fs}(r)$	0.90	0.342	536.3	534.6	0.6
$Q_g(r)$	0.95	0.111	544.9	534.6	1.2
$Q_{fhs}(r)$	0.90	0.098	549.3	534.6	1.4

\* - Q's correspond to those shown in first column.

### Corona Tests

The results of the corona tests show the effect of the corona wind on the heat transferred into the cavity. The effectiveness of the corona discharge on convection was determined by comparing the conduction through the heated phenolic plates for the two cases (with and without corona wind). For each configuration, the heat transfer rates,  $Q_{cav}$ , achieved with and without the corona wind are shown as well as the resulting flow patterns

inside the cavity.

Configuration #1. Table V shows the results of the corona tests for Configuration #1. In the table,  $T_{cav}(w/o)$  is the average temperature of the hot surface of the cavity without corona discharge and  $T_{cav}(with)$  is the average surface temperature with corona discharge. The temperature drop as a result of the corona wind,  $T_{cav}(drop)$ , is also shown in Table V.

The conduction rates with and without the presence of corona wind were calculated using the conduction equation, Equation (5). Table VI shows the heat transfer rates where  $Q_{cav}(w/o)$  represents the rate before corona wind and  $Q_{cav}(with)$  represents the rate while the corona wind was present. The table shows the transfer rates for positive and negative voltage potentials.

TABLE V  
Average Temperatures ( $^{\circ}F$ ) for Configuration #1

VOLTAGE	$T_{htr}$	$T_{cav}(w/o)$	$T_{cav}(with)$	$T_{cav}(drop)$
5kV(-)	160.9	152.7	151.7	1.0
5kV(+)	162.4	154.2	153.5	0.7
8kV(-)	160.3	152.1	147.5	4.6
8kV(+)	161.8	153.6	151.9	1.7
11kV(-)	160.7	152.5	143.7	8.8
11kV(+)	160.5	152.3	145.1	7.2
14kV(-)	159.9	151.7	142.0	9.7
14kV(+)	161.1	152.9	140.6	12.3

TABLE VI  
 $Q_{cav}$  Rates for Configuration #1

VOLTAGE	$Q_{cav}$ (w/o)	$Q_{cav}$ (with)	Ratio of $Q_{cav}$ 's
5kV (-)	12.7 BTU/hr	14.2 BTU/hr	1.1
5kV (+)	"	13.8 "	1.1
8kV (-)	"	19.8 "	1.6
8kV (+)	"	15.3 "	1.2
11kV (-)	"	26.3 "	2.1
11kV (+)	"	23.8 "	1.9
14kV (-)	"	27.7 "	2.2
14kV (+)	"	31.7 "	2.5

These results show corona effects increased the heat transfer rate by as much as 2.5 times the normal heat transfer rate. The general trends show that an increase in corona intensity (i.e., higher voltages) results in increased heat transfer rates. This result is similar with electrostatic cooling results of Franke (12,13) and Hogue (24) in that they also observed an increase in heat transfer rates as the voltage applied to the corona wires increased.

By monitoring the interferometer during testing, the flow patterns resulting from the corona discharge were determined. These patterns are shown in Fig. 9 for a positive voltage potential and in Fig. 10 for a negative voltage potential.

These patterns differ from the positive corona case in two ways. First, note that the flow over the lower surface was not reversed at 14kV as was the case for the positive corona. This may be due to the flow at the upper portion of the cavity having more influence over the flow at the lower

surface. Another difference from the positive corona tests was the reversal in the general flow patterns. This reversal is predicted in the text by Williams (25:49,50) in which he describes the corona discharge causing a net flow from the high voltage potential to the lower voltage potential. Although there is flow in both directions, the net effect is a flow from the higher potential to the lower. The flow at 5kV is different from the other voltages because the threshold voltage needed to create the corona effect had not been reached. This threshold voltage is lower for the negative potential than the positive potential. This was why the negative potential was more effective in cooling than the positive potential at the lower voltages.

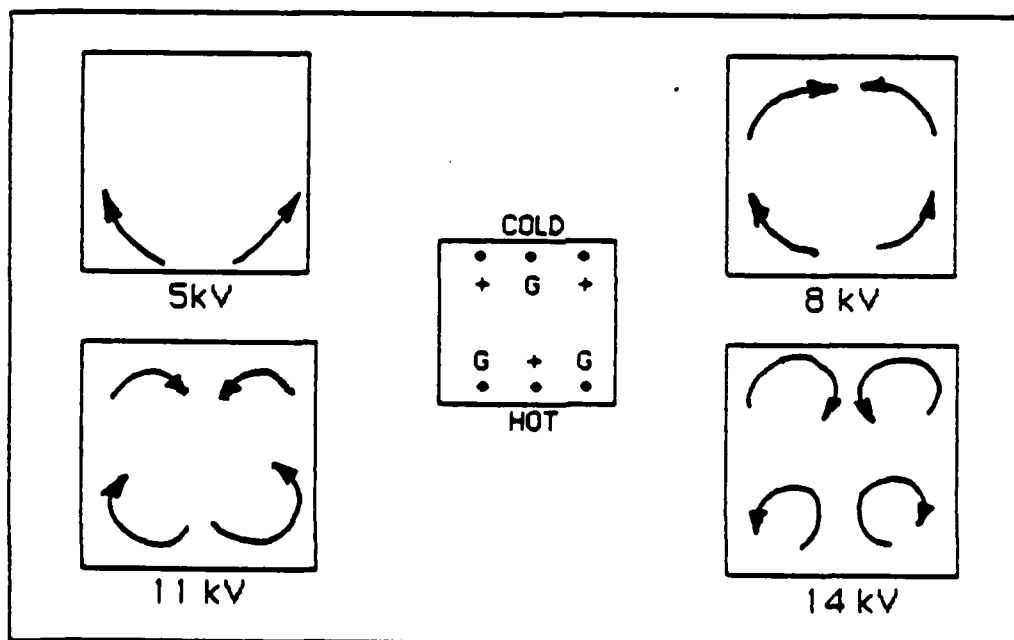


Fig. 9. Flow Patterns Resulting From Positive Voltage Potential for Configuration #1

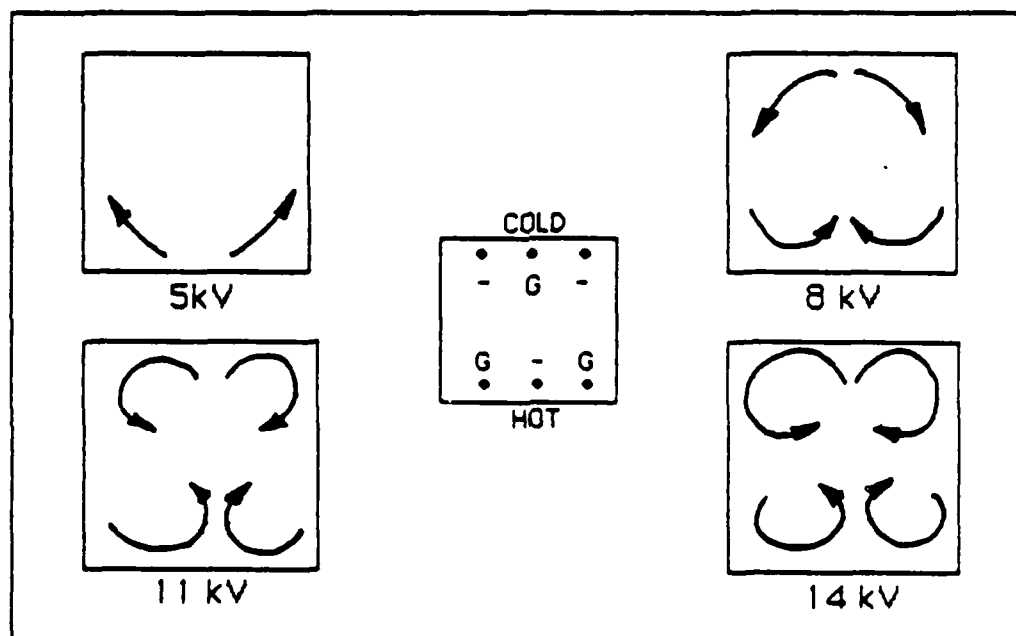


Fig. 10. Flow Patterns Resulting From Negative Voltage Potential for Configuration #1

Configuration #2 Table VII presents the average temperatures of the heaters and heated phenolic plates during tests using Configuration #2.

TABLE VII  
Average Temperatures ( $^{\circ}\text{F}$ ) for Configuration #2

VOLTAGE	$T_{\text{htr}}$	$T_{\text{cav}}(\text{w/o})$	$T_{\text{cav}}(\text{with})$	$T_{\text{cav}}(\text{drop})$
5kV(-)	162.3	154.1	153.2	0.9
5kV(+)	164.5	156.3	151.8	4.5
8kV(-)	161.9	153.7	150.1	3.6
8kV(+)	163.9	155.7	152.4	3.3
11kV(-)	161.7	153.5	146.8	6.7
11kV(+)	161.5	153.3	144.8	8.5
14kV(-)	161.3	153.1	145.7	7.4
14kV(+)	161.9	153.7	142.9	10.8

TABLE VIII  
 $Q_{cav}$  Rates for Configuration #2

VOLTAGE	$Q_{cav}$ (w/o)	$Q_{cav}$ (with)	Ratio of $Q_{cav}$ 's
5kV (-)	12.7 BTU/hr	14.1 BTU/hr	1.1
5kV (+)	"	19.6 "	1.5
8kV (-)	"	18.2 "	1.4
8kV (+)	"	17.8 "	1.4
11kV(-)	"	23.0 "	1.8
11kV(+)	"	25.8 "	2.0
14kV(-)	"	24.1 "	1.9
14kV(+)	"	29.4 "	2.3

The results show an increased heat transfer rate of up to 2.3 times the normal rate due to the corona cooling effect.

The resulting flow due to the corona wind for the positive potential corona tests are shown in Fig. 11. Although the patterns for 11kV and 14kV are identically depicted, the velocity of the corona wind at 14kV, through the interferometer, appeared to be greater than the velocity at 11kV. Also, the higher the voltage field, the more disturbed the flow appeared.

The negative potential case is depicted in Fig. 12. The flow patterns in this case were reversed from the flow using the positive potential. Again, as with the previous configuration, this reversal is consistent with the theory presented in the article by Williams (25:49,50). Namely, the effect of the corona discharge is a net flow from the higher potential to the lower.

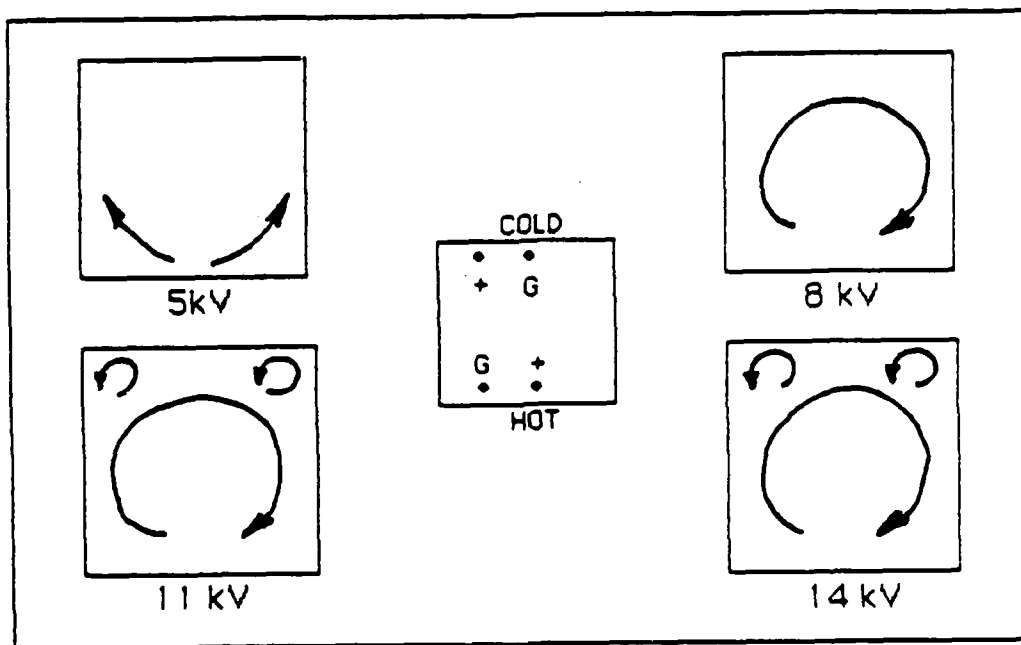


Fig. 11. Flow Patterns Resulting From Positive Potential for Configuration #2

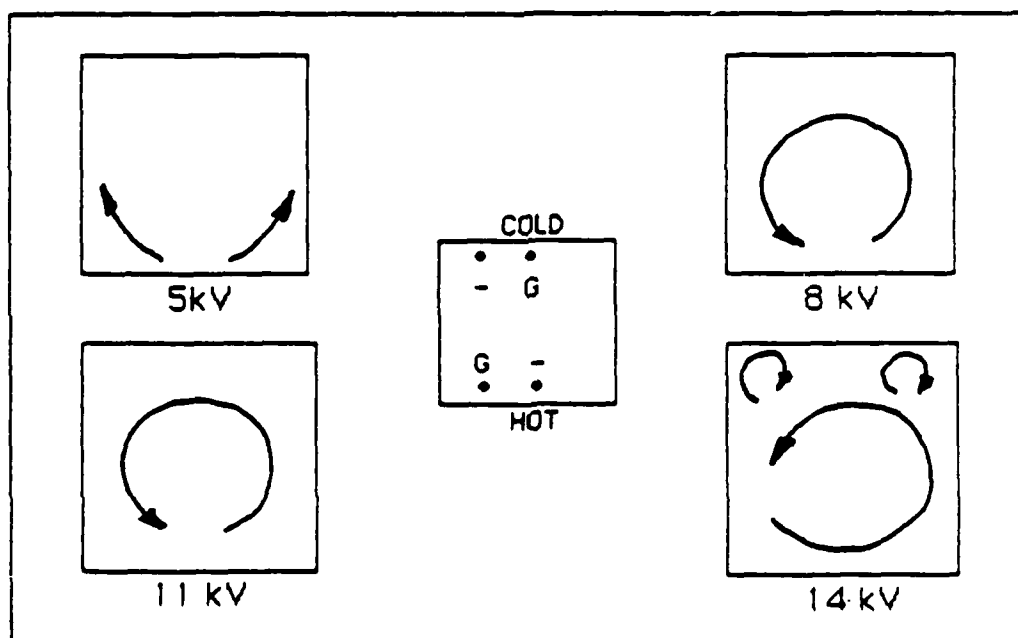


Fig. 12. Flow Patterns Resulting From Negative Potential for Configuration #2



Configuration #3. The average temperatures of the heaters and hot cavity surface are shown in Table IX and the conductive heat transfer rates are given in Table X.

TABLE IX  
Average Temperatures ( $^{\circ}\text{F}$ ) for Configuration #3

VOLTAGE	$T_{\text{htr}}$	$T_{\text{cav}}(\text{w/o})$	$T_{\text{cav}}(\text{with})$	$T_{\text{cav}}(\text{drop})$
5kV(-)	157.1	151.5	150.4	1.1
5kV(+)	157.1	151.5	151.1	0.4
8kV(-)	157.3	151.7	145.0	6.7
8kV(+)	157.3	151.7	149.5	2.2
11kV(-)	157.6	152.0	142.6	9.4
11kV(+)	155.4	149.8	145.3	4.5
14kV(-)	156.8	151.2	140.4	10.8
14kV(+)	157.7	152.1	140.5	11.6

TABLE X  
 $Q_{\text{cav}}$  Rates for Configuration #3

VOLTAGE	$Q_{\text{cav}}(\text{w/o})$	$Q_{\text{cav}}(\text{with})$	Ratio of $Q_{\text{cav}}$ 's
5KV (-)	8.6 BTU/hr	10.2 BTU/hr	1.2
5kV (+)	"	9.3 "	1.1
8kV (-)	"	19.0 "	2.2
8kV (+)	"	12.1 "	1.4
11kV(-)	"	23.2 "	2.7
11kV(+)	"	15.6 "	1.8
14kV(-)	"	25.3 "	2.9
14kV(+)	"	26.6 "	3.1

One of the major differences between this configuration and the previous two configurations was the heat transfer rate before corona was applied. The lower value of 8.64 Btu/hr was due to the decrease in the heat

transfer rate from the top of the cavity to the bottom. The heat conducted into the cavity was only two thirds that conducted when heating from below. This lower heat transfer rate resulted in higher percentage increases in heat transfer rates as compared to the previous configurations. As shown in Table X, heat transfer rates were tripled when corona wind was used to augment the heat transfer process.

The flow patterns inside the cavity using the positive voltage potential are shown in Fig. 13 while the patterns for the negative potential is given in Fig. 14. Again, the patterns using the positive potential are reversed from the negative potential flows. The flow inside the cavity also becomes more intense as the voltage potential between the corona wires is increased.

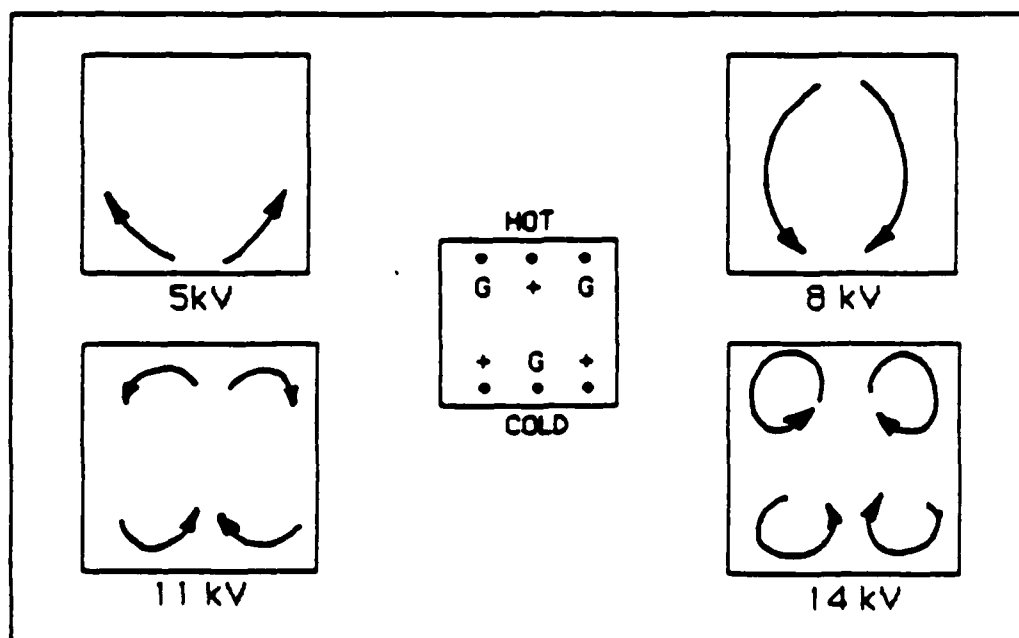


Fig. 13. Flow Patterns Resulting From Positive Voltage Potential for Configuration #3

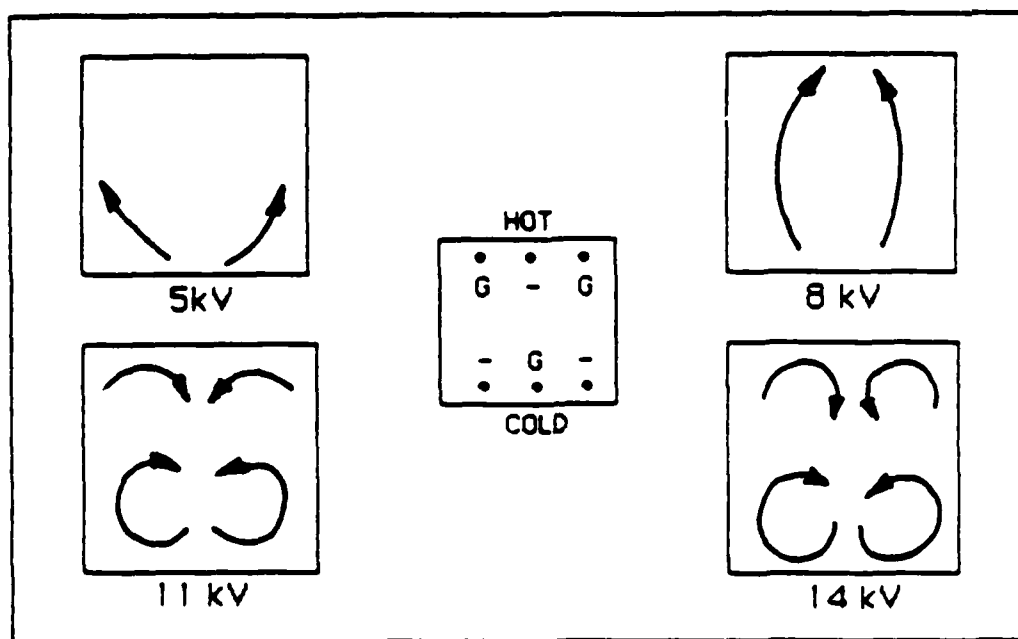


Fig. 14. Flow Patterns Resulting From Negative Voltage Potential for Configuration #3

Configuration #4. Table XI shows the average temperatures during the tests while Table XII gives the resulting heat transfer rates.

TABLE XI  
Average Temperatures ( $^{\circ}\text{F}$ ) for Configuration #4

VOLTAGE	$T_{\text{htr}}$	$T_{\text{cav(w/o)}}$	$T_{\text{cav(with)}}$	$T_{\text{cav(drop)}}$
5kV(-)	157.4	151.8	150.8	1.0
5kV(+)	158.5	152.9	152.5	0.4
8kV(-)	157.6	152.0	143.4	8.6
8kV(+)	158.7	153.1	150.5	2.6
11kV(-)	158.0	152.4	142.4	10.0
11kV(+)	157.6	152.0	145.3	6.7
14kV(-)	157.6	152.0	139.3	12.7
14kV(+)	157.6	152.0	137.6	14.4

TABLE XII  
Q<sub>cav</sub> Rates for Configuration #4

VOLTAGE	Q <sub>cav</sub> (w/o)	Q <sub>cav</sub> (with)	Ratio of Q <sub>cav</sub> 's
5kV (-)	8.6 BTU/hr	10.2 BTU/hr	1.2
5kV (+)	"	9.3 "	1.1
8kV (-)	"	21.9 "	2.5
8kV (+)	"	12.7 "	1.5
11kV(-)	"	24.1 "	2.8
11kV(+)	"	19.0 "	2.2
14kV(-)	"	28.3 "	3.3
14kV(+)	"	30.9 "	3.6

As noted in the Table XII, the corona wind increased transfer rates up to 3.5 times the rate achieved without the corona discharge. The general trends in these results are very similar to the results from Configuration #3; therefore, the discussion relating to those results applies to the results of this section.

For this configuration, the general flow patterns of the corona wind inside the cavity are depicted in the two figures, Figs. 15 and 16.

Figures 17 to 20 show the effect of corona wire voltage on Q<sub>cav</sub> for Configurations 1 through 4, Fig. 5. The positive potential was more effective at the higher voltages while the negative potential produced higher transfer rates at the lower voltages, except for Configuration 2, Fig. 18.

Configurations 3 and 4, shown in Figs. 19 and 20, use heating from above causing stratified air layers inside the cavity (i.e., conduction between the heated and cooled phenolic surfaces of the cavity). The introduction of corona wind into the cavity causes convection to take place within the

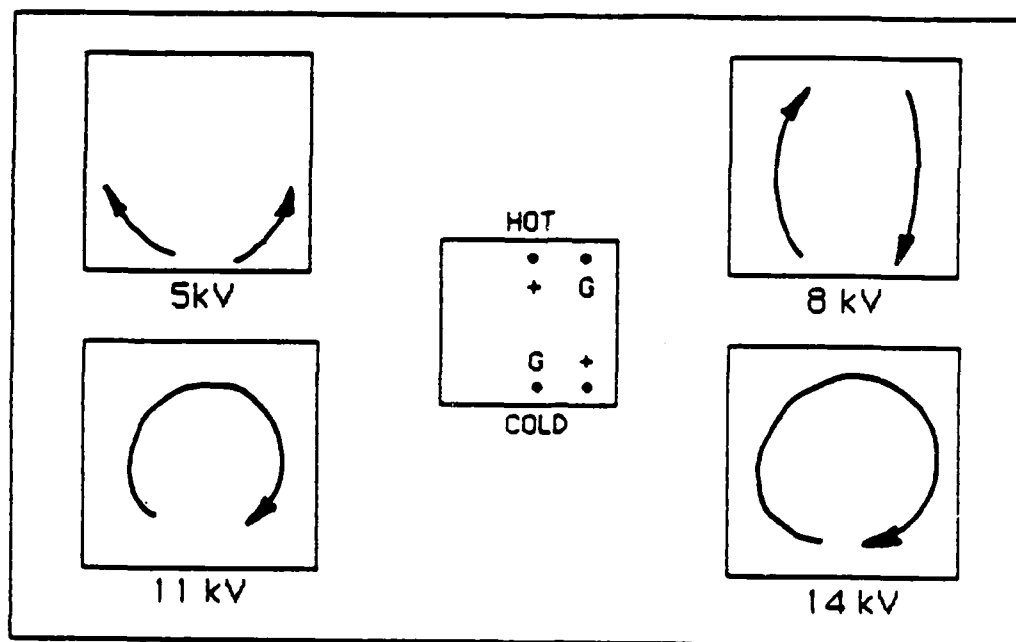


Fig. 15. Flow Patterns Resulting From Positive Potential for Configuration #4

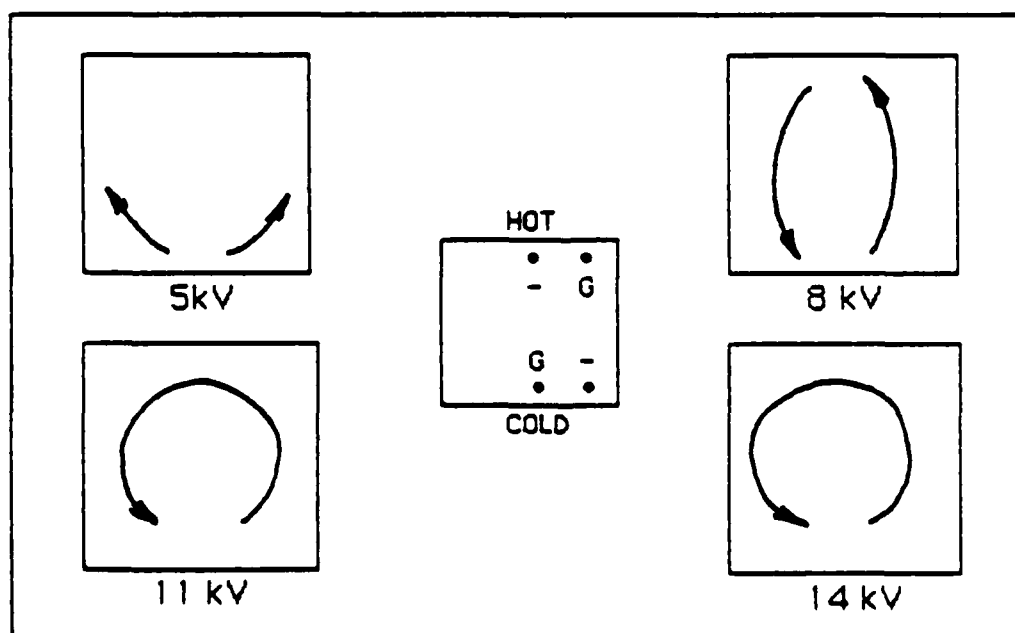


Fig. 16. Flow Patterns Resulting From Negative Potential for Configuration #4

cavity, thereby, significantly increasing the heat transferred away from the heated plate. Since the corona wind is more effective using a negative voltage potential at the lower voltages, this may explain the large gap in transfer rates between the negative and positive potentials in Figs. 19 and 20.

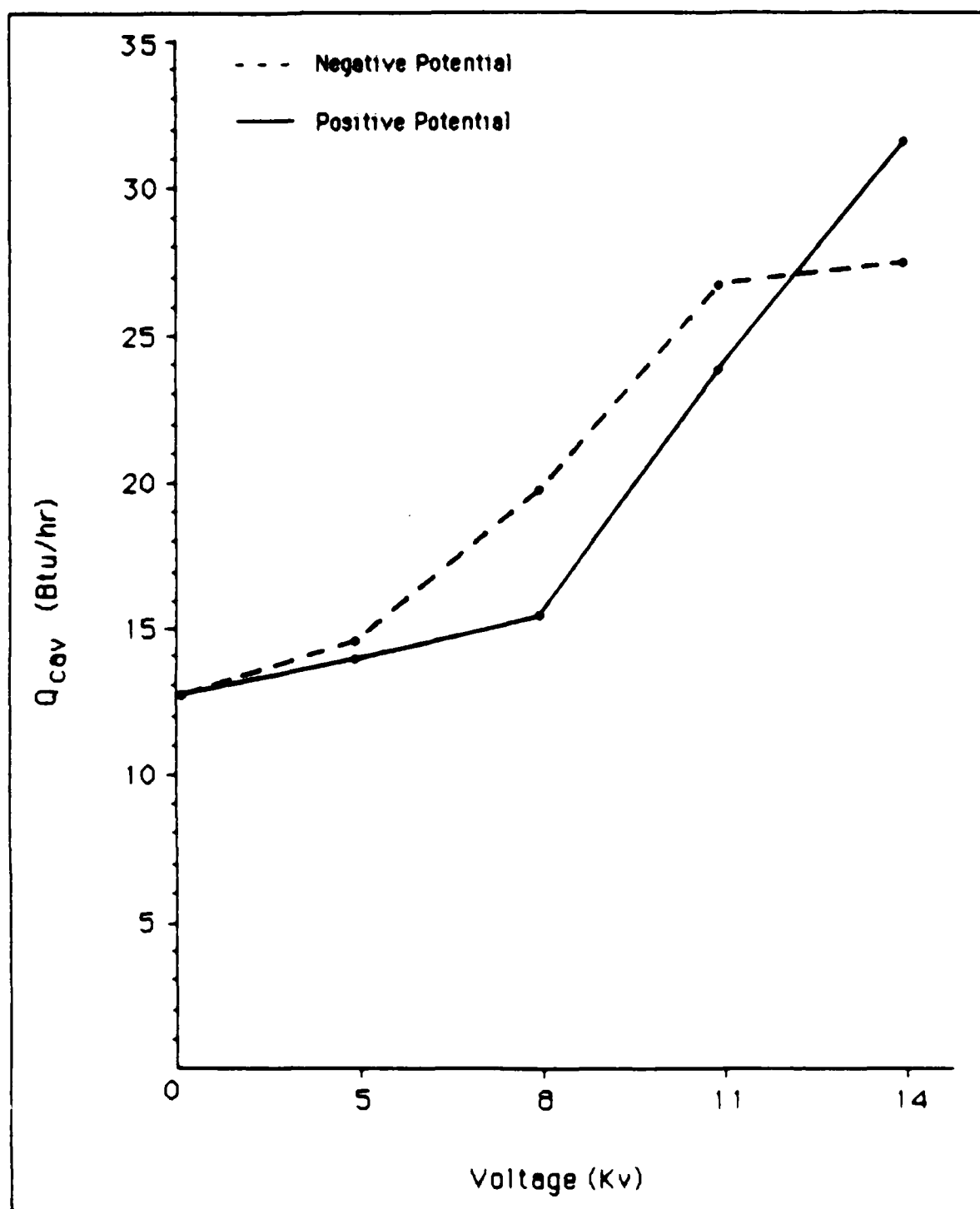


Fig. 17  $Q_{cav}$  vs Voltage for Configuration #1

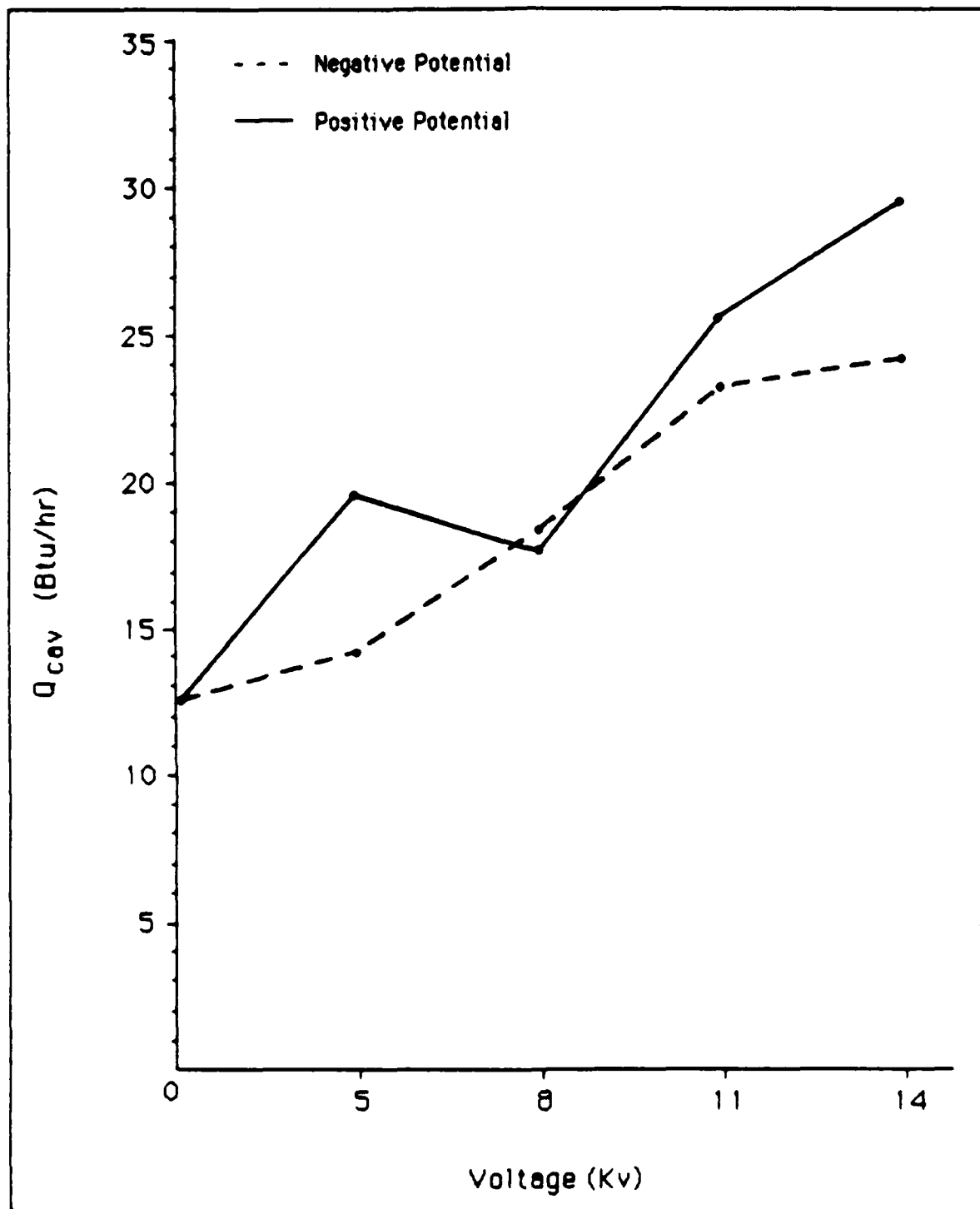


Fig. 18.  $Q_{cav}$  vs Voltage for Configuration # 2



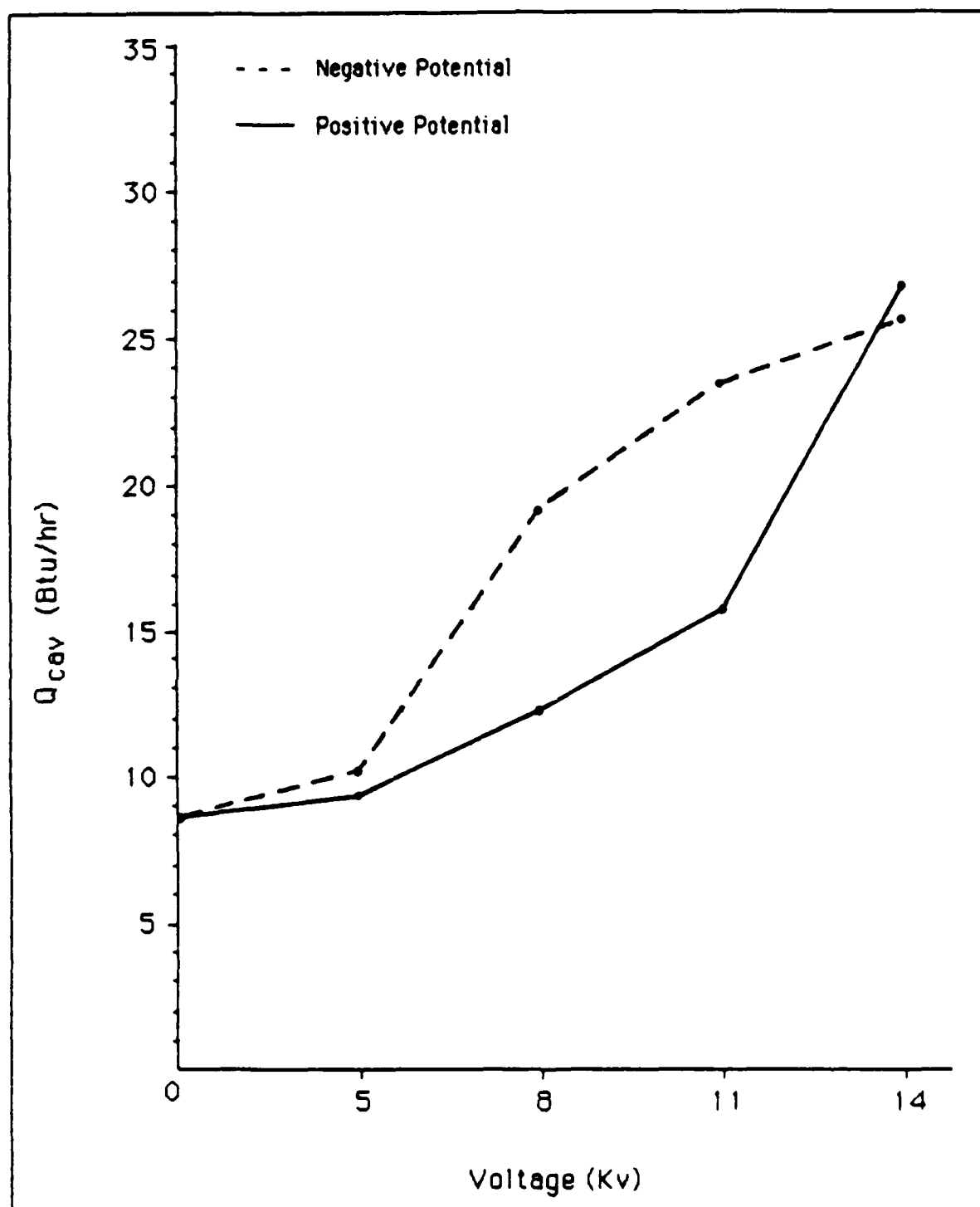


Fig. 19  $Q_{cav}$  vs Voltage for Configuration # 3

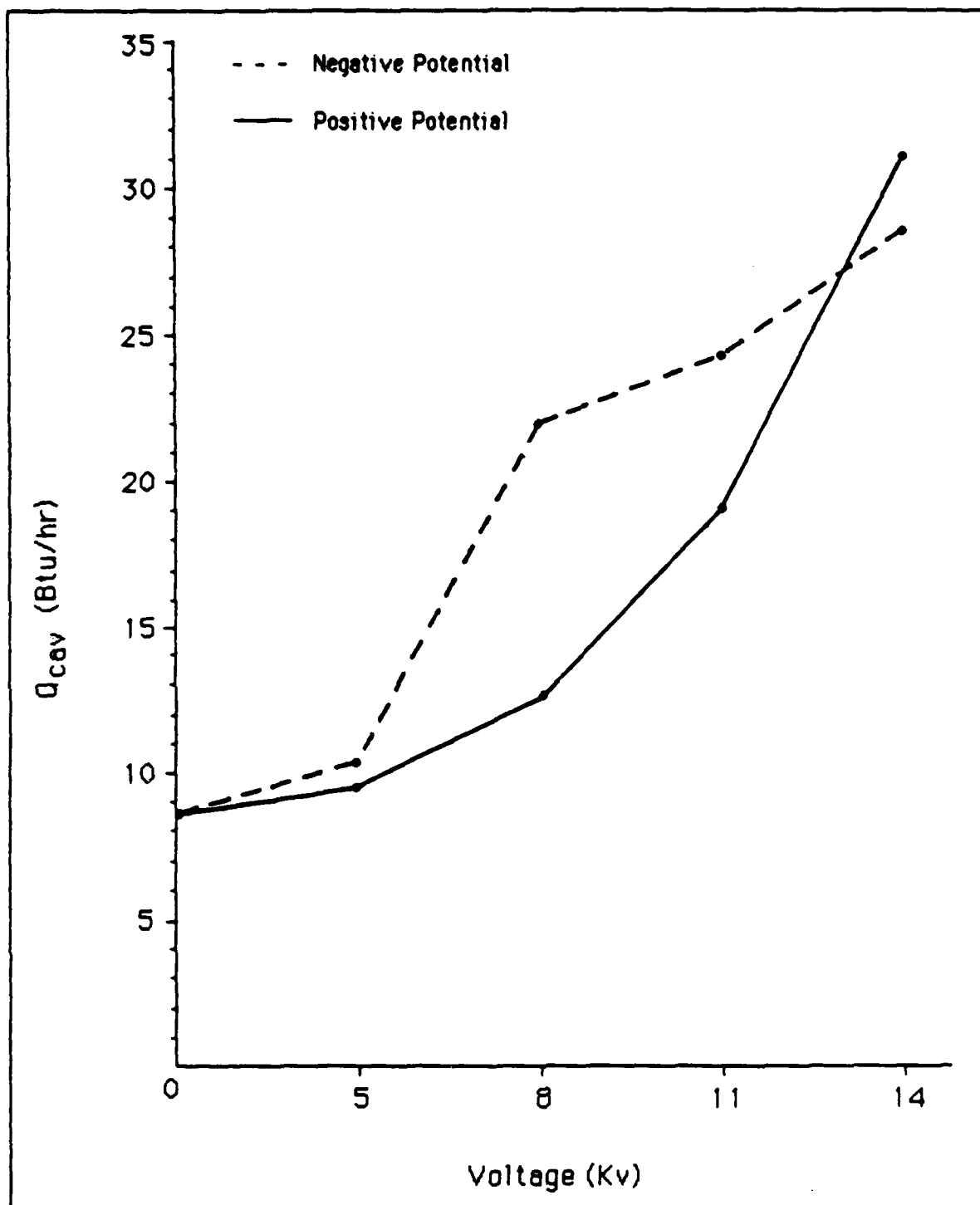


Fig. 20.  $Q_{cav}$  vs. Voltage for Configuration # 4

## VI. Conclusion

The basic conclusion of this study is heat transfer rates, on the hot side of a heated enclosure, can be increased when corona wind is established within the enclosure. It was shown that heat transfer rates for a heated surface of an enclosure can be increased as much as 3.5 times when a corona wind is introduced inside the enclosure.

There are other general conclusions that can be made based on the test results. At the lower voltages, the negative voltage potential was more effective than the positive voltage potential. However, at the higher voltages, the positive potential produced the higher heat transfer rates for the configurations tested. Finally, the heat transfer rate increases as the voltage applied to the corona wires are increased. This is true for both positive and negative corona.

## VII. Recommendations

There are several recommendations that would enhance understanding electrostatic cooling within an enclosure. These recommendations are:

1. Place numerous thermocouples near the heated surface of the cavity to determine which parts of the surface experience the greatest heat transfer rates.

2. Place thermocouples on all surfaces of the cavity to determine the effect the corona discharge has on the other surfaces.

3. Repeat the tests performed in this study with corona wires of a different material (e.g., alumel or nichrome wires).

4. Repeat the tests using a higher or lower temperature difference between the heated and cooled surfaces of the cavity. (The temperature differential in this study was 85 °F).

5. Use different gases inside the cavity and determine how this affects heat transfer rates.

6. Use different corona wire configurations to establish different flow patterns within the cavity.

7. Repeat the tests with the cavity inclined at various angles up to 90°.

These and other variations may shed more light on an area of study that has not had much research to date.

## References

1. Reynolds, R.E. and R.E. Holmes. "Heat Transfer in a Corona Discharge," Mechanical Engineering, 44-49 (Oct 1976).
2. Senftleben, H. "Die Einwirkung elektrischer and magnetischer Felder auf das Wärmeleitvermögen von Gasen," Phys. Z.S., 32: No.14 (1931).
3. Burke, S.P. "Heat Transfer," U.S. Patent 1835557, 1931.
4. Palueff, K.K. "Means for Cooling Electrical Apparatus," U.S. Patent 1980821, 1934.
5. Velkoff, H.R. Electrofluidmechanics: A Study of Electrokinetic Actions in Fluids, Aeronautical Systems Division, AFSC, Wright-Patterson AFB OH, Feb. 1962 (ASD-TR-61-642).
6. Velkoff, H.R. Electrofluidmechanics: Investigation of the Effect of Electrostatic Fields on Heat Transfer and Boundary Layers, Aeronautical Systems Division, AFSC, Wright-Patterson AFB OH, Sept. 1962 (ASD - TDR - 62 - 650).
7. Velkoff, H.R. "Effects of Electrostatic Fields on Fluid Flows," Proceedings Symposium on Fluidics and Internal Flows, Penn State Univ., University Park Pa., Oct 1968.
8. Velkoff, H.R. and J. Miller. The Effect of an Electrostatic Field on the Condensation of Vapor, Air Force Aero-Propulsion Laboratory, Wright-Patterson AFB OH, Feb 1964 (RTD-TDR-63-4008).
9. Velkoff, H.R. "The Effects of Ionization on the Flow and Heat Transfer of a Dense Gas in a Transverse Electric Field," Proceedings 1964 Heat Transfer and Fluid Mechanics Institute, 260-275. Stanford Univ. Press, Stanford Univ. CA, 1964.
10. Velkoff, H.R. and J. Miller. "Condensation Heat Transfer on a Vertical Plate with a Transverse Electric Field," ASME Journal of Heat Transfer, 87:197-201 (May 1965).

11. O'Brien, R.J. The Effect of an Electric Field on Heat Transfer from a Vertical Plate in Various Gases Over a Range of Pressures. MS Thesis, School of Engineering, Air Force Institute of Technology (AU), Wright-Patterson AFB OH, Aug. 1964.
12. Franke, M.E. "Effect of Vortices Induced by Corona Discharge on Free-Convection Heat Transfer From a Vertical Plate," Journal of Heat Transfer, 427-433 (Aug. 1967).
13. Franke, M.E., and K.E. Hutson. "Effects of Corona Discharge on Free Convection Heat Transfer Inside a Vertical Hollow Cylinder," ASME Journal of Heat Transfer, 106:346-351 (May 1984).
14. Velkoff, H.R. and F.A. Kulacki. "Electrostatic Cooling," ASME Design and Conference Show. Paper 77-DE-36. Chicago IL, May 9-12 1977.
15. Ostrach, S. "Natural Convection in Enclosures," Advances in Heat Transfer, Volume 8, 161-227. New York: Academic Press, 1972.
16. Batchelor, G.K. "Heat Transfer by Free Convection Across a Closed Cavity Between Vertical Boundaries at Different Temperatures," Quarterly of Applied Mathematics, 12:209-235 (1954).
17. Batchelor, G.K. "On Steady Laminar Flow with Closed Streamlines at Large Reynolds Number," Journal of Fluid Mechanics, 1:177-190 (1956).
18. Wilkes, J.O. The Finite Difference Computation of Natural Convection in an Enclosed Rectangular Cavity, Ph.D. Thesis, Univ. of Michigan, Ann Arbor MI, 1963.
19. Elder, J.W. "Laminar Free Convection in a Vertical Slot," Journal of Fluid Mechanics, 23: 77-98 (1965).
20. Vahl Davies, G. "Laminar Natural Convection in a Rectangular Cavity," International Journal of Heat and Mass Transfer, 11: 1675-1693 (1968).
21. Hsu, S.T. Engineering Heat Transfer. New York: Van Nostran Co., 1963.

22. Gochenaur, J.E. Investigation of Heat Transfer to a Turbine Blade Cascade Using a Shock Tube. MS Thesis, Air Force Institute of Technology, Wright-Patterson AFB OH, 1984.

23. Desmond, R.M. and B.V. Karlekar. Engineering Heat Transfer. New York: West Publishing Co., 1977.

24. Hogue, L.E. Effects of the Corona Wind on the Cooling of a Horizontal Cylinder. MS Thesis, Air Force Institute of Technology, Wright-Patterson AFB OH, 1984.

25. Williams, E.M. The Physics and Technology of Xerographic Processes. New York: John Wiley and Sons, 1978.

Appendix A

Tabulated Data



The following tables show the temperature readings of the eight thermocouples located on the hot and cold phenolic surfaces, Fig. 2. In the tables, NORMAL refers to measurements taken without the presence of the corona discharge and CORONA refers to measurements taken with the corona discharge. AMB represents the ambient room temperature measured approximately four feet away from the test cavity.

# DATA

CONFIGURATION: #1

VOLTAGE: 5kV (neg.)

## TEMPERATURES ( $^{\circ}$ F)

	HEATED SURFACE				COOLED SURFACE				AMB.
NORMAL	151.2	153.4	156.0	150.3	70.8	71.4	70.8	70.6	66.3
CORONA	151.0	152.5	153.6	149.8	70.5	71.1	70.0	69.8	

CONFIGURATION: #1

VOLTAGE: 5kV (pos.)

## TEMPERATURES ( $^{\circ}$ F)

	HEATED SURFACE				COOLED SURFACE				AMB.
NORMAL	152.4	155.3	157.7	151.4	72.2	72.9	72.4	72.4	67.5
CORONA	153.1	153.2	156.2	151.6	72.0	72.9	72.4	72.4	

CONFIGURATION: #2

VOLTAGE: 5kV (neg.)

## TEMPERATURES ( $^{\circ}$ F)

	HEATED SURFACE				COOLED SURFACE				AMB.
NORMAL	152.7	154.6	157.5	151.7	71.5	72.0	71.4	71.2	69.6
CORONA	151.6	155.2	155.7	150.2	70.7	71.4	70.3	70.4	

CONFIGURATION: #2

VOLTAGE: 5kV (pos.)

## TEMPERATURES ( $^{\circ}$ F)

	HEATED SURFACE				COOLED SURFACE				AMB.
NORMAL	154.5	157.6	159.6	153.4	72.0	72.1	72.0	71.7	69.0
CORONA	152.0	150.9	153.4	150.8	71.1	72.7	71.7	72.3	

DATA

CONFIGURATION: #3

VOLTAGE: 5kV (neg.)

TEMPERATURES ( $^{\circ}\text{F}$ )

	HEATED SURFACE				COOLED SURFACE				AMB.
NORMAL	150.4	154.0	154.0	147.4	68.5	67.5	67.4	67.4	68.8
CORONA	149.7	153.0	152.0	147.0	67.6	66.7	66.6	66.6	

CONFIGURATION: #3

VOLTAGE: 5kV (pos.)

TEMPERATURES ( $^{\circ}\text{F}$ )

	HEATED SURFACE				COOLED SURFACE				AMB.
NORMAL	150.2	154.1	154.0	147.5	68.8	67.8	67.7	67.8	68.8
CORONA	150.2	154.4	152.6	147.2	67.8	66.8	66.7	66.8	

CONFIGURATION: #4

VOLTAGE: 5kV (neg.)

TEMPERATURES ( $^{\circ}\text{F}$ )

	HEATED SURFACE				COOLED SURFACE				AMB.
NORMAL	150.6	154.4	154.4	147.8	68.5	67.5	67.5	67.5	69.2
CORONA	150.2	153.4	152.2	147.4	67.6	66.6	66.6	66.6	

CONFIGURATION: #4

VOLTAGE: 5kV (pos.)

TEMPERATURES ( $^{\circ}\text{F}$ )

	HEATED SURFACE				COOLED SURFACE				AMB.
NORMAL	151.7	155.6	155.4	148.8	69.0	67.8	67.8	67.8	69.1
CORONA	151.6	155.2	154.5	148.6	68.2	67.3	67.2	67.1	

# DATA

CONFIGURATION #1

VOLTAGE 8kV (neg)

TEMPERATURES ( $^{\circ}$ F)

	HEATED SURFACE				COOLED SURFACE				AMB
NORMAL	149.7	153.5	156.3	149.0	71.0	72.0	71.4	70.9	67.5
CORONA	148.0	145.8	148.4	147.7	71.0	71.9	71.0	71.4	

CONFIGURATION #1

VOLTAGE 8kV (pos)

TEMPERATURES ( $^{\circ}$ F)

	HEATED SURFACE				COOLED SURFACE				AMB
NORMAL	151.4	155.2	157.4	150.2	71.4	71.9	71.3	71.5	67.8
CORONA	150.2	153.5	155.2	148.6	70.6	72.7	72.0	70.9	

CONFIGURATION #2

VOLTAGE 8kV (neg)

TEMPERATURES ( $^{\circ}$ F)

	HEATED SURFACE				COOLED SURFACE				AMB
NORMAL	152.3	154.4	157.0	151.0	71.2	71.8	71.1	70.9	69.4
CORONA	152.2	151.5	150.4	146.2	71.4	72.6	70.9	70.0	

CONFIGURATION #2

VOLTAGE 8kV (pos)

TEMPERATURES ( $^{\circ}$ F)

	HEATED SURFACE				COOLED SURFACE				AMB
NORMAL	153.9	157.1	158.9	152.8	72.4	72.4	72.3	72.0	69.2
CORONA	151.6	152.0	154.7	151.4	70.8	72.5	72.9	72.9	

# DATA

CONFIGURATION: #3

VOLTAGE: 8kV (neg.)

## TEMPERATURES (°F)

	HEATED SURFACE				COOLED SURFACE				AMB
NORMAL	150.7	154.4	154.0	147.8	68.1	67.2	67.2	67.1	68.3
CORONA	145.8	146.0	144.9	143.3	67.6	67.3	68.2	66.5	

CONFIGURATION: #3

VOLTAGE: 8kV (pos.)

## TEMPERATURES (°F)

	HEATED SURFACE				COOLED SURFACE				AMB
NORMAL	150.4	154.6	154.0	147.6	68.0	67.2	67.0	67.1	68.4
CORONA	149.1	152.4	151.0	145.4	68.0	67.3	67.1	67.0	

CONFIGURATION: #4

VOLTAGE: 8kV (neg.)

## TEMPERATURES (°F)

	HEATED SURFACE				COOLED SURFACE				AMB
NORMAL	150.6	155.4	154.0	147.9	68.0	67.2	66.5	67.0	68.6
CORONA	144.3	146.1	142.1	141.2	66.6	67.2	68.1	66.8	

CONFIGURATION: #4

VOLTAGE: 8kV (pos.)

## TEMPERATURES (°F)

	HEATED SURFACE				COOLED SURFACE				AMB
NORMAL	151.7	155.8	155.8	149.1	68.9	68.0	68.0	67.8	69.2
CORONA	151.1	153.5	151.2	146.3	68.5	67.6	68.0	67.5	

# DATA

CONFIGURATION: #1

VOLTAGE: 11kV (neg.)

## TEMPERATURES (<sup>0</sup>F)

	HEATED SURFACE				COOLED SURFACE				AMB.
NORMAL	150.8	154.5	156.6	148.2	69.1	70.2	68.6	65.4	72.2
CORONA	144.8	143.6	145.2	141.3	70.4	70.0	68.0	65.0	

CONFIGURATION: #1

VOLTAGE: 11kV (pos.)

## TEMPERATURES (<sup>0</sup>F)

	HEATED SURFACE				COOLED SURFACE				AMB.
NORMAL	152.4	153.5	155.5	147.7	73.0	73.2	71.4	68.2	72.2
CORONA	145.7	145.6	147.5	141.6	73.2	75.1	71.4	66.0	

CONFIGURATION: #2

VOLTAGE: 11kV (neg.)

## TEMPERATURES (<sup>0</sup>F)

	HEATED SURFACE				COOLED SURFACE				AMB.
NORMAL	154.0	155.0	156.8	148.4	73.1	73.2	71.2	68.0	72.3
CORONA	149.4	146.6	147.7	143.4	70.9	73.0	73.4	68.2	

CONFIGURATION: #2

VOLTAGE: 11kV (pos.)

## TEMPERATURES (<sup>0</sup>F)

	HEATED SURFACE				COOLED SURFACE				AMB.
NORMAL	153.5	154.6	156.6	148.4	72.8	72.9	70.8	67.6	72.5
CORONA	148.6	145.4	144.9	140.5	73.4	73.2	71.2	66.3	

# DATA

CONFIGURATION: #3

VOLTAGE: 11kV (neg.)

## TEMPERATURES ( $^{\circ}$ F)

	HEATED SURFACE				COOLED SURFACE				AMB.
NORMAL	150.8	153.0	154.8	147.5	69.0	67.8	67.6	67.6	67.2
CORONA	143.3	144.1	142.2	140.8	69.5	68.2	68.0	66.4	

CONFIGURATION: #3

VOLTAGE: 11kV (pos.)

## TEMPERATURES ( $^{\circ}$ F)

	HEATED SURFACE				COOLED SURFACE				AMB.
NORMAL	147.6	154.1	152.6	145.0	72.2	71.1	71.4	71.1	66.7
CORONA	145.2	148.6	146.4	140.8	71.6	71.1	70.5	69.9	

CONFIGURATION: #4

VOLTAGE: 11kV (neg.)

## TEMPERATURES ( $^{\circ}$ F)

	HEATED SURFACE				COOLED SURFACE				AMB.
NORMAL	151.8	155.2	154.7	148.0	69.5	68.2	68.0	68.0	69.3
CORONA	144.1	143.4	141.6	140.7	67.5	68.7	69.8	67.8	

CONFIGURATION: #4

VOLTAGE: 11kV (pos.)

## TEMPERATURES ( $^{\circ}$ F)

	HEATED SURFACE				COOLED SURFACE				AMB.
NORMAL	151.4	154.7	154.2	147.8	68.7	67.7	67.7	67.5	69.2
CORONA	147.1	147.8	145.1	141.1	69.1	67.8	68.0	66.8	

DATA

CONFIGURATION: #1

VOLTAGE: 14kV (neg.)

TEMPERATURES ( $^{\circ}$ F)

	HEATED SURFACE				COOLED SURFACE				AMB.
NORMAL	150.7	154.4	155.2	146.6	75.0	74.4	72.4	69.7	72.4
CORONA	141.8	144.8	144.2	137.2	73.3	78.1	73.2	66.5	

CONFIGURATION: #1

VOLTAGE: 14kV (pos.)

TEMPERATURES ( $^{\circ}$ F)

	HEATED SURFACE				COOLED SURFACE				AMB.
NORMAL	151.1	154.4	157.1	149.2	71.9	72.2	71.3	69.2	72.6
CORONA	139.6	144.0	143.6	135.4	71.7	75.9	71.9	67.2	

CONFIGURATION: #2

VOLTAGE: 14kV (neg.)

TEMPERATURES ( $^{\circ}$ F)

	HEATED SURFACE				COOLED SURFACE				AMB.
NORMAL	153.2	154.6	156.1	148.4	73.5	73.7	72.0	68.8	72.0
CORONA	147.5	147.0	147.4	140.9	72.2	73.9	74.0	67.9	

CONFIGURATION: #2

VOLTAGE: 14kV (pos.)

TEMPERATURES ( $^{\circ}$ F)

	HEATED SURFACE				COOLED SURFACE				AMB.
NORMAL	153.9	155.0	156.9	149.0	74.1	74.1	72.5	69.3	72.1
CORONA	146.4	143.4	143.2	138.6	72.6	73.3	72.1	72.0	



# DATA

CONFIGURATION: #3

VOLTAGE: 14kV (neg.)

## TEMPERATURES (<sup>0</sup>F)

	HEATED SURFACE				COOLED SURFACE				AMB.
NORMAL	150.3	153.8	153.6	147.1	70.1	68.7	68.3	68.3	67.5
CORONA	141.0	142.8	140.6	137.3	69.6	71.0	69.5	65.4	

CONFIGURATION: #3

VOLTAGE: 14kV (pos.)

## TEMPERATURES (<sup>0</sup>F)

	HEATED SURFACE				COOLED SURFACE				AMB.
NORMAL	151.1	154.8	154.7	147.8	70.5	68.8	68.6	68.5	67.5
CORONA	140.0	143.5	141.8	136.9	68.6	70.9	69.6	67.2	

CONFIGURATION: #4

VOLTAGE: 14kV (neg.)

## TEMPERATURES (<sup>0</sup>F)

	HEATED SURFACE				COOLED SURFACE				AMB.
NORMAL	151.3	154.5	155.2	147.0	69.3	68.0	66.7	66.5	71.8
CORONA	140.3	141.6	140.9	134.5	67.9	69.8	68.2	64.6	

CONFIGURATION: #4

VOLTAGE: 14kV (pos.)

## TEMPERATURES (<sup>0</sup>F)

	HEATED SURFACE				COOLED SURFACE				AMB.
NORMAL	150.6	154.4	155.6	147.2	67.6	66.8	65.6	65.8	72.0
CORONA	139.5	139.9	137.8	133.1	65.1	67.9	67.7	65.1	

Appendix B

Photographs of Test Equipment



Fig. 21. Photograph of Test Object

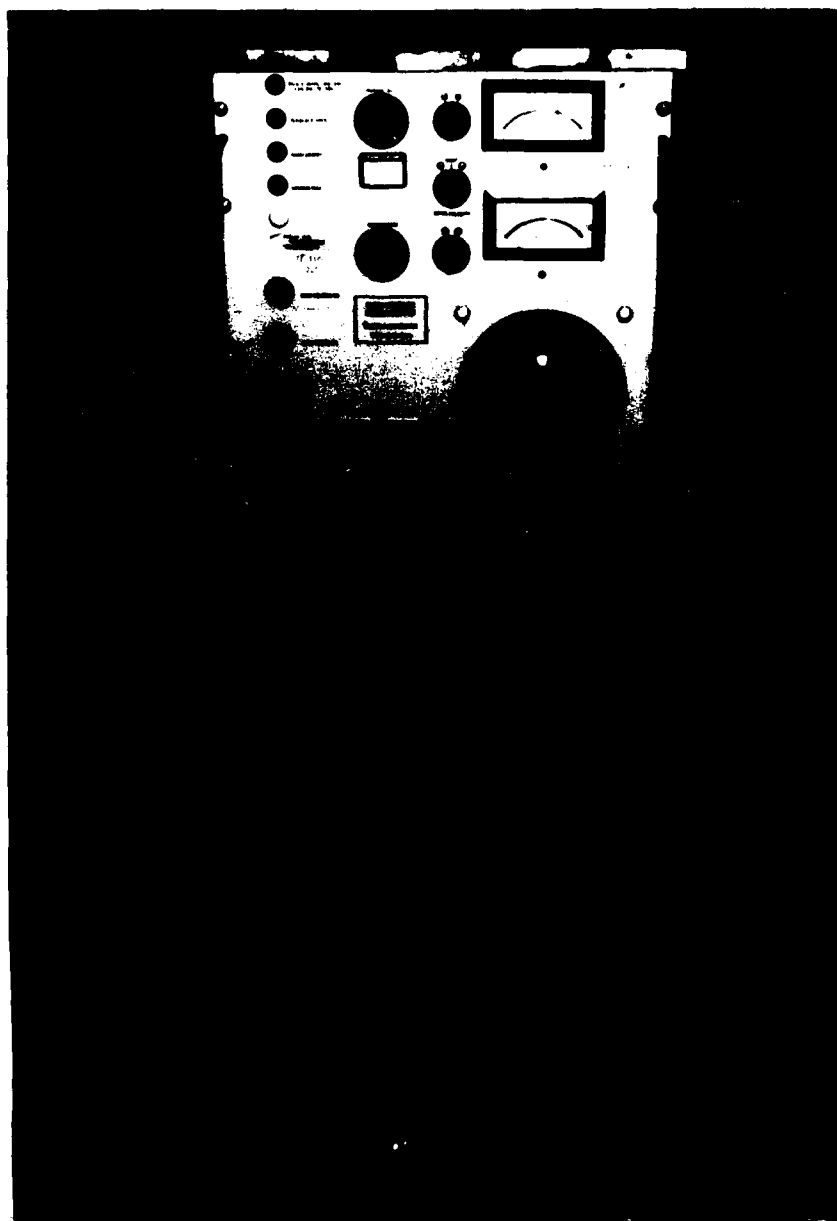


Fig. 22. Picture of High Voltage Power Supply



Fig. 23. Picture of Transformer Used to Adjust Heater Plate Current

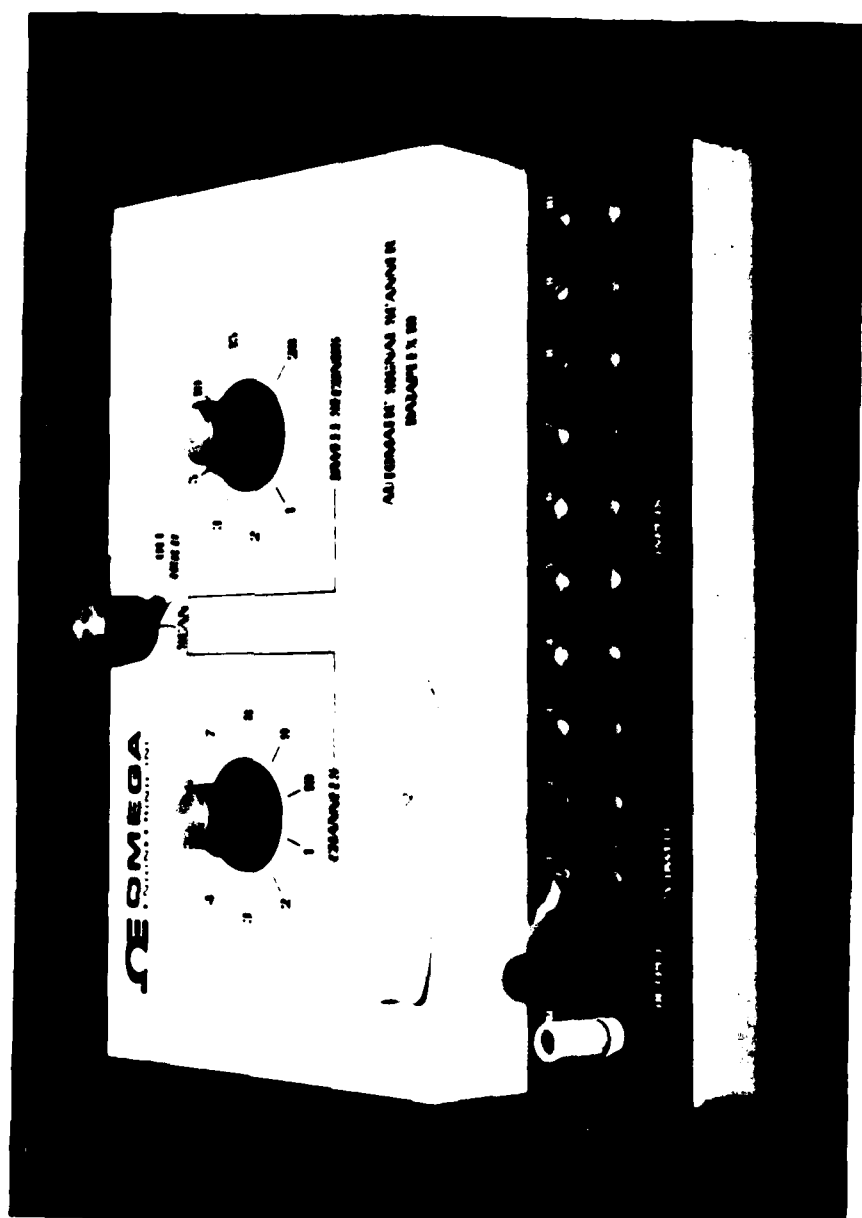


Fig 24 Photograph of Digital Scanner for Thermocouples



Fig 25 Photograph of Temperature Measuring Unit Used to  
Take Thermocouple Readings

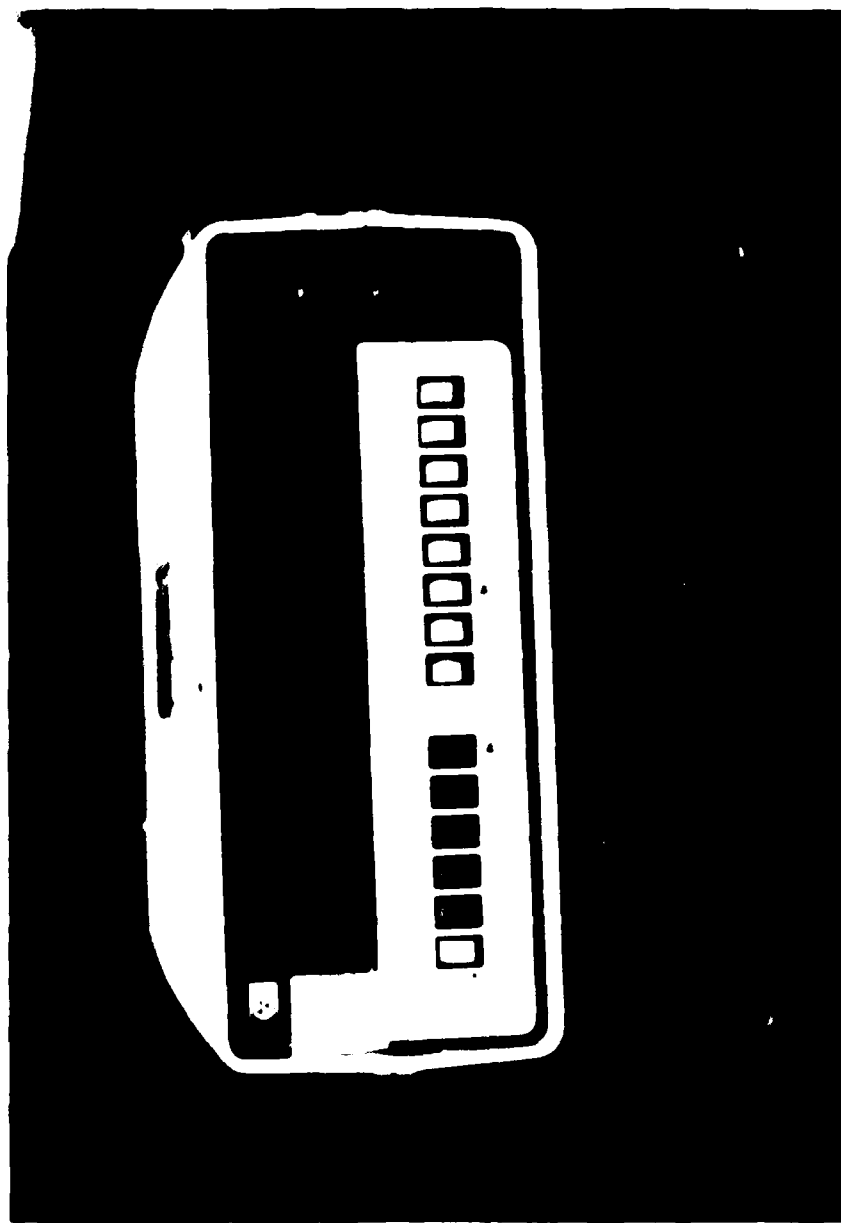


Fig 26 Picture of Digital Multimeter Used to Measure Heater  
Plate Currents



Appendix C

Interferometer Alignment

## Interferometer Alignment

The alignment of a Mach-Zehnder interferometer can be a laborious process unless one uses a convergent alignment process. The process used in this study was one described by Gochenaur (22:75-78) and was proven to be a useful, time-saving technique. The procedure is presented for the benefit of those who may need to work with a Mach-Zehnder interferometer. The components described in this section are depicted in Figure 3 on p. 9.

In order to see the interference fringes, the two beams of light (one beam through the reference section and the other beam through the test section) need to be parallel. Therefore, before one begins to adjust the mirrors or splitter plates, the interferometer itself should be leveled. To complete the rest of the alignment procedure, a telescope-like device was used to look through the interferometer in order to monitor the effects of any mirror or splitter plate adjustments.

The telescope was used to align the images of two objects located between the illumination mirror,  $m_{illum}$ , and the first splitter plate,  $Sp_1$ . One of the objects was a thermocouple wire stretched just in front of  $Sp_1$  and the second object was the illumination mirror itself. When the telescope was focused on the illumination mirror, it appeared as a double image. The mirror was brought into focus using rotation knob #3 for horizontal control and control knob #4 for vertical control. Next, the telescope was focused on the thermocouple wire, which also first appeared as a double image. This time the image was brought together using control knob #1 for horizontal movement and control knob #2 for vertical

movement. The telescope was refocused on the illumination mirror and then on the thermocouple wire, each time using the control knobs to bring the double image into a single image. The procedure was repeated until both objects appeared as a single image without having to move the control knobs.

Once the initial control settings were established, the fringes could be seen somewhere within the range of focus of the telescope. The fringes could be positioned most anywhere within the interferometer using horizontal adjustments to splitter plate 2 (control knob #1). Clockwise rotations caused the fringes to move toward the telescope while counter-clockwise rotations caused the fringes to move away. As a result, it was relatively easy to center the fringe patterns at the test section.

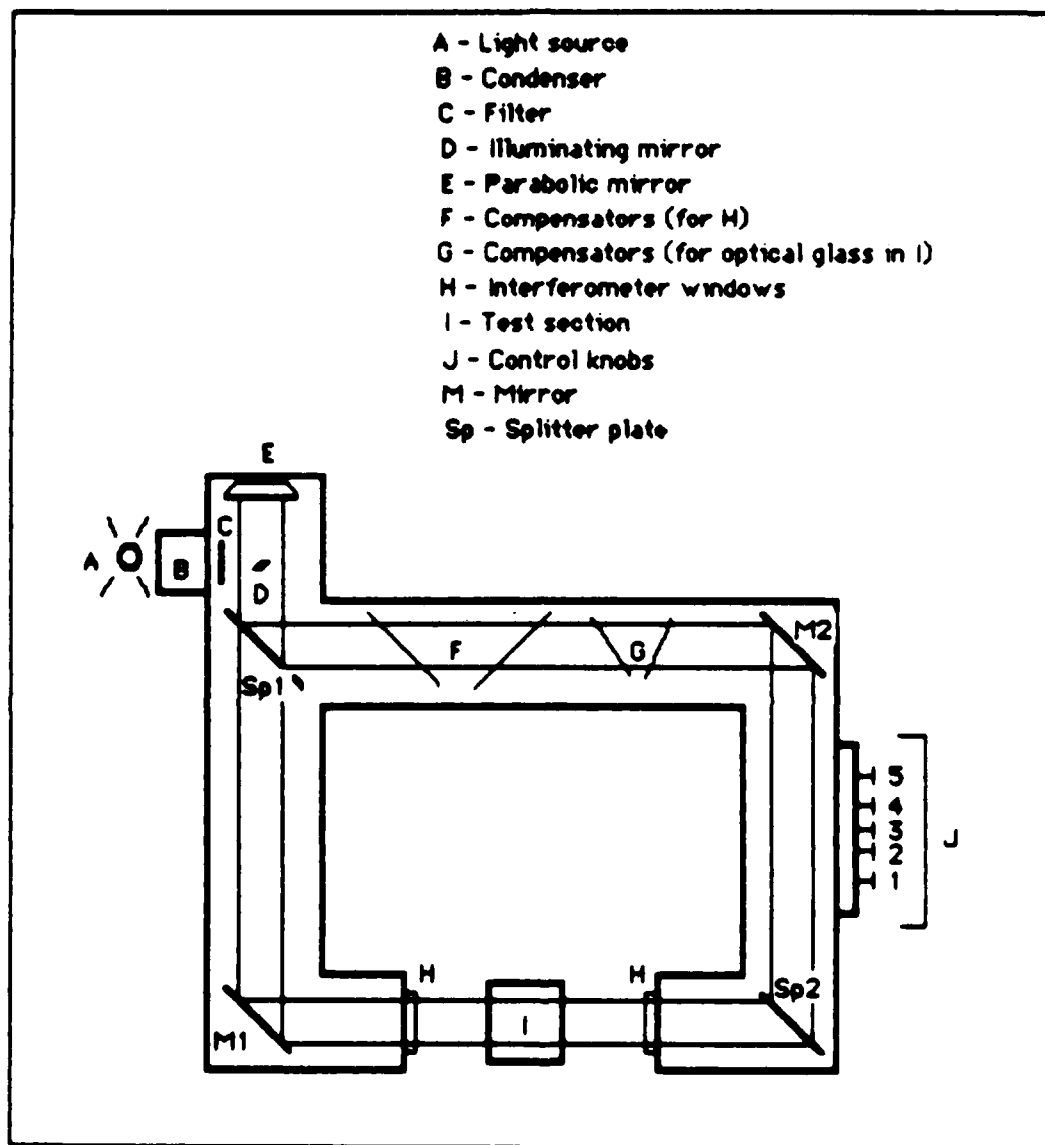


Fig. 27. Mach-Zehnder Interferometer

## VITA

Captian Donald D. Dyer, Jr. was born [REDACTED] PII Redacted  
In 1973, he graduated from [REDACTED] and entered Auburn University. He received a Bachelor of Aerospace Engineering degree and was commissioned into the U.S. Air Force in 1977. In 1978, Capt Dyer was awarded navigator wings and completed flying training in the RF-4C at Shaw AFB, S.C.. He served as a Weapon System Officer (WSO) at Kadena AB, Japan and, upon his return from overseas, attended Squadron Officer School in residence. Capt Dyer was then assigned to Bergstrom AFB, Tx. as an instructor WSO and, while at Bergstrom, received a Master of Science in Management degree from Houston Baptist University. His jobs included chief of scheduling for the 45 Tactical Reconnaissance Training Squadron and chief of the Radar Training and Sensors Branch for the 67 Tactical Reconnaissance Wing. He entered the Air Force Institute of Technology in May 1984.

Permanent Address: [REDACTED]  
[REDACTED]

PII Redacted

AD A179-209

## REPORT DOCUMENTATION PAGE

1a. REPORT SECURITY CLASSIFICATION <b>UNCLASSIFIED</b>		1b. RESTRICTIVE MARKINGS	
2a. SECURITY CLASSIFICATION AUTHORITY		3. DISTRIBUTION/AVAILABILITY OF REPORT Approved for public release; distribution unlimited.	
2b. DECLASSIFICATION/DOWNGRADING SCHEDULE			
4. PERFORMING ORGANIZATION REPORT NUMBER(S) <b>AFIT/GA/AA/86D-4</b>		5. MONITORING ORGANIZATION REPORT NUMBER(S)	
6a. NAME OF PERFORMING ORGANIZATION <b>School of Engineering</b>	6b. OFFICE SYMBOL (If applicable) <b>AFIT/EN</b>	7a. NAME OF MONITORING ORGANIZATION	
6c. ADDRESS (City, State and ZIP Code) <b>Air Force Institute of Technology Wright-Patterson AFB, OH 45433</b>		7b. ADDRESS (City, State and ZIP Code)	
8a. NAME OF FUNDING/SPONSORING ORGANIZATION	8b. OFFICE SYMBOL (If applicable)	9. PROCUREMENT INSTRUMENT IDENTIFICATION NUMBER	
8c. ADDRESS (City, State and ZIP Code)		10. SOURCE OF FUNDING NOS.	
		PROGRAM ELEMENT NO.	PROJECT NO.
		TASK NO.	WORK UNIT NO.
11. TITLE (Include Security Classification) <b>See Box 19</b>			
12. PERSONAL AUTHOR(S) <b>Donald D. Dyer, Jr., B.S., M.S.M., Capt. USAF</b>			
13a. TYPE OF REPORT <b>MS Thesis</b>	13b. TIME COVERED FROM _____ TO _____	14. DATE OF REPORT (Yr., Mo., Day) <b>1986 December</b>	15. PAGE COUNT <b>76</b>
16. SUPPLEMENTARY NOTATION			
17. COSATI CODES		18. SUBJECT TERMS (Continue on reverse if necessary and identify by block number)	
FIELD	GROUP	SUB. GR.	
		Heat Transfer	
		Corona Discharge	
		Enclosures	
19. ABSTRACT (Continue on reverse if necessary and identify by block number)			
Title: <del>ENCLOSURE CORONA COOLING FOR ENCLOSURES</del> <i>see title Page</i>			
Thesis Chairman: <b>Dr. Milton E. Franke</b> Professor of Mechanical Engineering			
<div>Approved for public release: LAW AFR 190-1. <i>Lyn E. Wilson</i> 13 MAR 87 LYN E. WILSON Dean for Research and Professional Development Air Force Institute of Technology (AFIT) Wright-Patterson AFB OH 45433</div>			
20. DISTRIBUTION/AVAILABILITY OF ABSTRACT UNCLASSIFIED/UNLIMITED <input checked="" type="checkbox"/> SAME AS RPT. <input type="checkbox"/> DTIC USERS <input type="checkbox"/>		21. ABSTRACT SECURITY CLASSIFICATION <b>UNCLASSIFIED</b>	
22a. NAME OF RESPONSIBLE INDIVIDUAL <b>Dr. Milton E. Franke</b> Professor of Mechanical Engineering	22b. TELEPHONE NUMBER (Include Area Code) <b>513-255-2362</b>	22c. OFFICE SYMBOL <b>AFIT/ENY</b>	

Experiments were conducted to determine the effects of corona wind on heat transfer rates for enclosures. Tests were performed with an enclosed cavity heated on the bottom and cooled on the top (and vice-versa). A corona wind was established inside the cavity by applying high voltages to 0.004 inch diameter chromel wires placed along the hot and cold surfaces of the cavity. Tests were conducted using both positive voltage potential and negative voltage potential to create the corona discharge. Different wiring configurations were used to establish a variety of flow patterns inside the cavity.

The heated surface heat transfer rates were calculated for each of the test configurations with and without corona. These heat transfer rates were determined when the corona discharge was present and compared to the rates found when the discharge was not present. Comparing these transfer rates revealed how much the corona wind augmented the heat transfer process. Results showed corona wind can increase heat transfer rates inside an enclosure by almost four times the rates attained without the corona discharge for the wire configurations investigated. (T10:25)